7-7-2015

Stability Analysis and Novel Control Concepts for Multiple Time-delay Systems

Qingbin Gao
University of Connecticut - Storrs, qingbin.gao@uconn.edu

Stability Analysis and Novel Control Concepts for Multiple Time-delay Systems

Qingbin Gao, Ph.D.

University of Connecticut, 2015

Systems with delays exist universally in engineering, such as manufacturing process, networked control systems, tele-operation of robots, multi-robot systems, internal combustion engines, and traffic dynamics. Delays are ubiquitously observed in these systems due to the unavoidable time, which is required to gather information needed for decision-making, to generate control decisions, and to execute these decisions. These delays are crucial factors that may deteriorate or even destabilize the performance of the controlled systems. A critical question is: *How to design controllers so that these time-delayed control systems can tolerate larger delays?* To answer this, we first explore the interplay between the stability and the performance features of the systems under the presence of multiple delays. This pathway leads to the ultimate objective of devising effective and efficient algorithms to analyze the stability of systems with multiple delays, and designing controllers for such systems, so that their stability can be guaranteed against larger delays and their performance can be optimized, in spite of the potential adverse effects of delays.

As a result of this research, two control strategies were proposed for this class of systems: “Sign Inverting Control (SIC)” and “Delay Scheduling Control (DSC)”. Sign Inverting Control is a novel control strategy to increase the delay-robustness capability of the system against larger delays. It starts from an existing nominal control logic (such as linear-quadratic regulator, LQR) formulated for non-delayed dynamics and simply inverts the sign of the control gains. The selection option between the nominal and Sign Inverting control schemes render a more robust

control performance against much larger delay variations than each of the schemes. The other control logic, Delay Scheduling Control, is an unusual and interesting control concept, which suggests to increase the existing delays intentionally to improve the control performance, such as recovering the lost stability and increasing the disturbance rejection speeds. Such a multi-faceted and paradoxical combination of control logics provides previously-unexplored tools to the controller designers.

Stability Analysis and Novel Control Concepts for Multiple Time-delay Systems

Qingbin Gao

B.S., Harbin Institute of Technology, 2011

A Dissertation

Submitted in Partial Fulfillment of the

Requirements for the Degree of

Doctor of Philosophy

at the

University of Connecticut

2015

APPROVAL PAGE

Doctor of Philosophy Dissertation

Stability Analysis and Novel Control Concepts for Multiple Time-delay Systems

Presented by
Qingbin Gao, B.S.

Major Advisor

_____

Nejat Olgac

Associate Advisor

_____

Jiong Tang

Associate Advisor

_____

Chengyu Cao

Associate Advisor

_____

Bi Zhang

Associate Advisor

_____

Horea Ilies

University of Connecticut

2015

Acknowledgements

First and foremost, I would like to express my sincere gratitude to my major Ph.D. advisor, Professor Nejat Olgac, for his exceptional support, guidance and encouragement throughout my four years' stay in the ALARM (Advanced Laboratory for Automation, Robotics and Manufacturing) research group. I am very grateful to him for providing such a nice place to study, to learn and to grow with some great colleagues who care about each other. Without them, this Ph.D. thesis along with several novel publications in the control community that we have would never exist. It has always been a great pleasure and honor for me to work with such an advisor who is very enthusiastic and keen in research and who has spent lots of his time and energy supervising me and helping me grow to be an independent researcher. I am also very grateful to Professors Jiong Tang, Chengyu Cao, Bi Zhang and Horea Ilies for their continuous review and supervision of my progress through my entire Ph.D. program.

This work has been supported in part by grants from Army Research Office (Grant No. W911NF-07-1-0557) and the National Science Foundation (CMS-0539980).

I wish to thank my colleagues in the ALARM Lab, and they are Umut Zalluhoglu, Ayhan Kammer, Dr. Rudy Cepeda-Gomez, and Dr. Zhenyu Zhang, for sharing with me their knowledge, experience and enthusiasm in research. I have a lot of good memories with each one of them and I appreciate their effort in creating such an enjoyable working environment during my Ph.D study in the ALARM lab. Special thanks go to Umut Zalluhoglu and Ayhan Kammer for their valuable time, in assisting me to set up the experiments, identifying the system parameters, implementing time delayed control on the setup and conducting various experiments. I would also like to thank Dr. Rudy Cepeda-Gomez for supervising me as a senior graduate student and serving as a role model for young scholars like me to follow. I am also greatly indebted to Dr. Zhenyu Zhang for those fruitful discussions and invaluable sharing of research experience.

Finally, I owe the successful completion of this work to my father Wanwen Gao and my mother Shuying Ge, who have always been supporting me emotionally and financially in almost every stage of my life. Their unlimited and unconditional love always serves to encourage me to go for what I want and to follow my heart. I would like to dedicate this humble work to them.

Qingbin Gao, June 7th, 2015

Table of Contents

List of Figures

List of Tables

1. Introduction and Problem Statement

1.1 Introduction

Delays exist universally in engineering, such as manufacturing process [1], networked control systems [2], tele-operation of robots [3], multi-robot systems [4], internal combustion engines [5], and traffic dynamics [6]. Delays are ubiquitously observed in these so-called time-delay systems due to the unavoidable time required to gather sensing data needed for decision-making, to generate control decisions, and to execute these decisions. These delays are crucial factors that may deteriorate or even destabilize the performance of the systems. Due to these undesired and dangerous effects of time delays in the dynamics, the stability analysis of time-delay systems becomes mandatory at the beginning of the system design stage. Therefore, the stability robustness of linear time invariant time-delay systems (LTI-TDS) has been a major concern for over five decades, yielding a respectable volume of literature ([7-9] [10-12]). A major research topic in this class is the parametric stability analysis of these systems within the space of the delay(s). The determination of the robustness for such systems against uncertainties in delay and other system parameters is also widely studied ([13, 14] [15, 16] [17, 18] [19, 20]). A major focus of the cutting-edge research has been on the development of tools and methods that enable stability analysis of these systems. Such efforts resulted in various numerical methods [14, 15, 17-19], and an analytical procedure of the authors' research group, Cluster Treatment of Characteristic Roots (CTCR) [21, 22]. CTCR is, in fact, a paradigm that imparts a method to assess stability of LTI-TDS. The LTI-TDS have infinitely many characteristic roots due to its infinite dimension. Among these infinitely many roots, there are also infinitely many imaginary roots with specific delay compositions for a certain system. These infinite delay compositions constitute a bunch of hypersurfaces in the domain of the delays, on which the LTI-TDS have an imaginary characteristic roots. For this dynamics, it was found out that there are only a finite number of "kernel" hypersurfaces which can generate their infinitely many "offspring"

hypersurfaces. In addition, starting from points on the "kernel" and their corresponding "offspring" hypersurfaces and increasing only one of the delays infinitesimally while keeping all the other delays fixed, the direction of the movement of the imaginary roots remains identical. The novelty of the CTCR paradigm lies under these two observations with detailed mathematical explanation in Appendix A.

In addition to the stability analysis, the authors' group spent considerable effort on the control synthesis for LTI-TDS. Such studies resulted in the development of several concepts including Delay Scheduling Control (DSC) and Sign Inverting Control (SIC). Earlier development of DSC is discussed in several publications leading to [23] which handles multiple-delay cases with experimental validations. The article [24], on the other hand, is the only archival document on SIC. It presents the preliminary development on the concept which treats the class of dynamics with a single delay only. For both SIC and DSC operations, as well as for the stability paradigm CTCR, an important attribute is the 'large delays'. By 'large' we mean that the delays encountered in the operation are in the order of magnitude of the period of the fastest controlled dynamics. Say, for a desired trajectory which has 10 Hz as the highest frequency content, this study is focusing on control feedback delays in the order of 10^{-1} s (sec). The practical implication of this point is that small delays (such as a few sampling periods) are not of concern. On the contrary, this line of study investigates cases which bring much longer sensing and actuation delays, characterized as 'feedback delays'.

Before proceeding further, we make some notational remarks that are used in the entire thesis. The letter i represents the complex number $\sqrt{-1}$, unless mentioned otherwise. $\Re^{k+}$ represents a k-dimensional vector with members of positive (for the plus symbol) real numbers, while a $k \times k$ real matrix is denoted by $\Re^{k\times k}$. Boldface notation is used for vector and matrix quantities, while scalars are in regular face. The scalar elements of a vector, $\{\boldsymbol{a}\}$, are denoted as $\{\boldsymbol{a}\} = (a_1, a_{2,} \ldots)$. $\dot{\mathbf{x}}$ is used for

the first derivative of vector **x** with respect to time, dx/dt. Right (and left) half open complex plane.

1.2 Problem Statement

We start with a general class of linear time-invariant systems

$$\dot{\mathbf{x}} = \mathbf{A}\mathbf{x} + \overline{\mathbf{B}}\mathbf{u} \tag{1.1}$$

where $\mathbf{x}$ $(n\times 1)$ is the state vector, $\mathbf{u}$ $(m\times 1)$, $m \le n$ is the control input, $\mathbf{A}$ and $\overline{\mathbf{B}}$ are matrices of appropriate dimensions. The conventional full-state feedback control logic is taken as $\mathbf{u} = -\sum_{i=1}^{l} \mathbf{K}_i \mathbf{x}(t-\tau_i)$

where, $\mathbf{K}_i, i = 1,2,...,l$ $(m\times n)$ are the feedback gain matrices and $\tau_i, i = 1,2,...,l$ are the delays occurring in the feedback lines. The dynamics of the system becomes:

$$\dot{\mathbf{x}} = \mathbf{A}\mathbf{x} + \sum_{i=1}^{l} \mathbf{B}_i \mathbf{x}(t-\tau_i) \tag{1.2}$$

where $\boldsymbol{\tau} = (\tau_1, \tau_2, ..., \tau_l) \in \Re^{l+}$, $\mathbf{B}_i = -\overline{\mathbf{B}}\mathbf{K}_i, i = 1,2,...,l$. The system in (1.2) is known as linear time-invariant multiple time-delay systems (LTI-MTDS). The characteristic equation for this system is:

$$CE(s, \boldsymbol{\tau}) = \det(s\mathbf{I} - \mathbf{A} - \textstyle\sum_{i=1}^{l} \mathbf{B}_i e^{-\tau_i s}) \tag{1.3}$$

where s is the characteristic roots. It is well known that this system represents a globally asymptotically stable dynamics when all of its infinite spectra lie in the left-half of the complex plane. For a given selection of "original" feedback control structure, $\mathbf{B}_i, i = 1,2,...,l$ the CTCR paradigm provides a non-conservative and exhaustive stability picture in the domain of the delays, $\boldsymbol{\tau} = (\tau_1, \tau_2, ..., \tau_l) \in \Re^{l+}$. Each delay value is independent from each other, i.e.,

$$\tau_i / \tau_j \in \overline{Q}, \; i \neq j, \;\; i = 1, 2, \ldots p, \;\; j = 1, 2, \ldots p \tag{1.4}$$

rendering (1.3) to be a multiple time delayed system (MTDS). Therefore, the general form of (1.3) is called LTI-MTDS.

The dynamics in (1.3) can be regarded as a representation of LTI dynamics with multiple time delays or a nonlinear system linearized at a certain equilibrium operating point, which is commonly performed in engineering under reasonable assumptions. In general, the matrix $\mathbf{A}$ denotes the state matrix, whose eigenvalues determine the natural response characteristics of the uncontrolled dynamics

$$\dot{\mathbf{x}} = \mathbf{A}\,\mathbf{x}$$

while $\mathbf{B}_i\mathbf{x}(t-\tau_i)$ represents the feedback control on the system above, but with feedback line contaminated with time delays, τ_i. It should be noted that the uncontrolled dynamics itself, without any feedback control, may possess inherent time delays, in case of which the general LTI-MTDS of (3) is also encountered.

The characteristic equation of the system in (1.3) can be rewritten as

$$CE(s,\boldsymbol{\tau}) = \det\left[s\mathbf{I} - \mathbf{A} - \sum_{j=1}^{p}\mathbf{B}_j e^{-\tau_j s}\right] = A_0(s) + A_{p+1}(s,\tau_1,\ldots,\tau_p) + \sum_{j=1}^{p} e^{-n_j\tau_j s} A_j(s,\tau_1,\ldots,\tau_{j-1},\tau_{j+1},\ldots,\tau_p) \tag{1.5}$$

$A_0(s)$ is an n^{th} degree polynomial in s, A_j's $(j=1\ldots p)$ are quasi-polynomials in s and all the delays except τ_j. n_j is the highest order of commensuracy of delay τ_j, i.e. $n_j = rank\,(\mathbf{B}_j)$, in the dynamics $(n_j \le n)$. $A_0(s)$ is free of delays and it carries the highest power of s, s^n term, qualifying (1.2) as 'retarded' LTI-MTDS. A_{p+1} is another quasi-polynomial which contains all the remaining terms with lower commensuracy levels (in τ_j) than n_j, $j=1\ldots p$. In short, A_j's are the factors multiplying the representative exponential of the highest commensuracy of τ_j, i.e., $e^{-n_j\tau_j s}$.

The parametric stability analysis of the LTI-MTDS (1.3) within the space of the delay(s) and other system parameters have been widely studied ([13, 14] [15, 16] [17, 18] [19, 20]). A major research topic has been on the development of tools that enable stability analysis of these systems. Such efforts resulted in various numerical methods [14, 15, 17-19], and an analytical procedure of the authors' research group, Cluster Treatment of Characteristic Roots (CTCR) [21, 22]. CTCR is, in fact, a practical and universally applicable methodology, which assesses the stability robustness of LTI-MTDS (1.3) against multiple time delays. That is, the objective is to obtain the complete stability robustness picture in the semi-infinite domain of $\boldsymbol{\tau} = (\tau_1, \tau_2, ..., \tau_l) \in \Re^{l+}$ space with exact stability boundaries in $\boldsymbol{\tau}$, while all the other system parameters are fixed. CTCR starts from the exhaustive determination of stability boundaries in the domain of the delays. Contrary to the frequent misconception, the CTCR paradigm is transparent to the methodology which evaluates these hypersurfaces. A broad range of clever procedures in the literature can determine them [21, 22, 25, 26]. The extended Kronecker summation methodology is used in [21] to reduce the infinite-dimensional problem to an eigenvalue problem. As a result, the computational time is shortened considerably in determining these hypersurfaces, compared with conventional algorithms. The "building block" concept is introduced to the time-delay system for the first time in [22]. As a consequence, this concept yields a very practical and numerically efficient procedure in determining the stability hypersurfaces in the domain of the delays. The paper [25] proposes a methodology of explicit and complete parameterization and geometric characterization of the stability crossing set of linear systems with three delays. In [26], the crossing set, consisting of all the frequencies corresponding to all the points in the stability crossing curves, are expressed in terms of simple inequality constraints and are easily identified from the gain response curves of the coefficient transfer functions of the delay terms. Furthermore, it is found that these curves may be closed curves, open ended curves, and spiral-like curves oriented horizontally, vertically, or diagonally, and the category of these curves is determined in this thesis. Using the information of these stability hypersurfaces, CTCR produces a crisp (i.e. non-conservative) and exhaustive declaration of stable regions in the domain of the delays. We name this stability-based partitioning in the delay space the 'stability map' of the system.

In this thesis, the first chapter starts with an extensive review of the methodologies in the stability analysis of time delayed systems. This presentation is followed by the introduction of two control schemes for the time delayed systems with multiple delays, i.e., Sign Inverting Control (SIC) and Delay Scheduling Control (DSC). Chapter 2 introduces several ways for the exhaustive determination of marginal stability operating points, across which the stability of the system may be changed. In Chapter 3, two control schemes, SIC and DSC are explained in detail for LTI-MTDS. In Chapter 4, we outline a strategic procedure for the optimization of SIC so that the delay robustness and control performance are optimized. Chapter 5 introduces experimental cases to verify the proposed control schemes. Finally, Chapter 6 states the conclusion of the work done and declares some directions for future research that have been opened. For the sake of completeness, and to avoid interruptions in the logic flow of the text, the CTCR methodology is described in the Appendix A.

2. Exhaustive Determination of Operating Points with Marginal Stability

2.1 Kernel and Offspring Hypercurves

In order to determine the stability picture of the LTI time-delayed system, we utilize the CTCR paradigm, which is previewed in this section. The main aim of CTCR is the determination of the *number of unstable characteristic roots* (*NU*) over $\boldsymbol{\tau} \in \Re^{l+}$ domain. As per the D-Subdivision theorem (or the "root continuity argument") [27], the change of *NU* only occurs along certain loci within the domain of the delays where at least one pair of imaginary roots exists. Therefore, the CTCR methodology requires an exhaustive detection of these loci. Among various techniques to obtain them we follow an approach which is presented in a new domain, spectral delay space (SDS) [22]. Relevant definitions and crucial propositions of CTCR and SDS are highlighted in the following paragraphs without proofs, borrowing from [22, 28, 29].

We define the complete set of the *imaginary* spectra of the dynamics in (1.3) for all possible delays $\boldsymbol{\tau} \in \Re^{l+}$ as

$$\begin{aligned} \boldsymbol{\Omega} &= \{\omega_c \mid CE(s=\omega_c i, \boldsymbol{\tau}) = 0, \;\; \boldsymbol{\tau} \in \Re^{l+}, \;\; \omega_c \in \Re^{+}\} \\ &= \{\omega_c \mid <\boldsymbol{\tau}, \omega_c>, \;\; \boldsymbol{\tau} \in \Re^{l+}, \;\; \omega_c \in \Re^{+}\} \end{aligned} \tag{2.1}$$

where $<\boldsymbol{\tau}, \omega_c>$ indicates that for a $\boldsymbol{\tau} \in \Re^{l+}$, there exists an imaginary root, $\omega_c i$, of (1.3). With this notation we classify the stability switching boundaries that correspond to $<\boldsymbol{\tau}, \omega_c>$ occurrences into two classes:

Definition 1: Kernel Hypercurves (KH) $\wp_0^{DS}$ **:** The curves that consist of *all* the points $\boldsymbol{\tau} \in \Re^{l+}$ exhaustively, which cause an imaginary root and satisfy the constraint $0 < \tau_k \omega_c < 2\pi$ (k=1, 2,…, l) are called the *kernel hypercurves*. The points on this curve contain the smallest delay compositions which correspond to all possible imaginary roots. By its definition, the kernel hypercurves formation is unique for a given characteristic equation (1.3). The characteristic equation (1.3) possess imaginary roots along *countably infinite* number of hypercurves. Mathematical representation of this set is

$$\wp_0^{DS} = \{\boldsymbol{\tau} = (\tau_1, \tau_2, ..., \tau_l) \,|\, CE(\omega_c i, \boldsymbol{\tau}) = 0, \omega_c \in \Re^+, 0 \le \boldsymbol{\tau}\omega_c < 2\pi\} \tag{2.2}$$

■

Definition 2: Offspring Hypercurves (OH) $\wp^{DS}$ **:** The hypercurves obtained from the kernel hypercurves by the following point-wise nonlinear transformation:

$$\left\langle \tau_1 \pm \frac{2\pi}{\omega_c} j_1, \tau_2 \pm \frac{2\pi}{\omega_c} j_2, ..., \tau_l \pm \frac{2\pi}{\omega_c} j_l \right\rangle, \quad j_1, j_2, ..., j_l = 0,1,2,\ldots \tag{2.3}$$

are called the *offspring hypercurves*. This definition simply utilizes the fact that any point on the *kernel* will result in ∞^l (l dimensional infinity) *offspring.* ■

2.2 Spectral Delay Space Domain and Building Block Concept

2.2.1 Definitions

Spectral Delay Space (SDS) and the Building Block (BB) concept are proposed in a recent thesis work [30] and also the author's paper [22]. They provide a numerically efficient algorithm to determine the stability hypersurfaces for LTI time-delay systems. We now recite the properties of Spectral Delay Space (SDS) domain and Building Block (BB) concept, which prepare readers a background for the main contribution of this chapter.

Spectral Delay Space (SDS): A new procedure is described in this segment for determining the kernel (and offspring) curves. The procedure is developed on a new domain: SDS. It is defined by the coordinates $v_j = \tau_j \omega_c$ for every point $\boldsymbol{\tau} = (\tau_1, \tau_2, ..., \tau_l) \in \Re^{l+}$ on the kernel and the offspring curves. This is a conditional mapping: if a delay set $\boldsymbol{\tau} = (\tau_1, \tau_2, ..., \tau_l)$ creates an imaginary root $\pm\omega_c i$, then

$\boldsymbol{\tau}\omega_c = (\tau_1\omega_c, \tau_2\omega_c, ..., \tau_l\omega_c)$ forms a point in the SDS. On the contrary, delay points that do not generate an imaginary root have no representation in the SDS since they are not important from the stability stand point.

The main advantage of SDS is that the representation of the kernel curve in the SDS, denoted as $\wp_0^{SDS}$ and called the ***building curve***, is confined into a l dimensional cube of edge length 2π. Then, it is only necessary to explore a finite domain to find the representation of the building curves in the SDS. This finite domain is known as the *building block* (BB)**,** i.e., a l dimensional cube, as per (2.2). Another advantage of these coordinates is that the transitions from the *building* to the *reflection* curves (i.e., the representation of the *offspring* curves in the SDS) is achieved simply by stacking the copies of the BB as opposed to using the point-wise non-linear transformation (2.3), which results in an undesirable shape distortion. There are several other intriguing properties of the SDS and BB concepts which can be found in the work of [22]. Here, we introduce a few of them without proof.

Property 1: **Kernel isolation property.** The BB contains no trace of reflection curves in the SDS.

Property 2: The building curves end on the surface of the BB or close onto themselves inside the BB.

Property 3: **Symmetricity property of building curves.** The point $(\pi, \pi, ..., \pi)$ in SDS is the centre of symmetry of the BB as well as the building curves. For each $<\boldsymbol{\tau}, \omega_c>$ set in the building block, there is also a $<\boldsymbol{\tau}, -\omega_c>$ set, which are symmetric with respect to the point $(\pi, \pi, ..., \pi)$. The proof is available in the work of [22].

2.2.2 Stability Charts in Delay Space and Root Tendency

For the ease of conveyance and formalism, a system with two independent delays is considered from now on in the Chapter 2.2

$$\dot{\mathbf{x}} = \mathbf{A}\mathbf{x} + \mathbf{B}_1\mathbf{x}(t-\tau_1) + \mathbf{B}_2\mathbf{x}(t-\tau_2) \tag{2.4}$$

where $rank(\mathbf{B}_1) = rank(\mathbf{B}_2) = 1$, $rank(\mathbf{B}_1 + \mathbf{B}_2) = 2$. The discussion in the following part of this chapter is given for systems in this state space form; however, they can be easily extended to more complicated systems with more than two delays and additional commensurate delays. The class of characteristic equations considered here is

$$\begin{aligned} CE_\tau(s,\tau_1,\tau_2) &= a_0(s) + a_1(s)e^{-\tau_1 s} + a_2(s)e^{-\tau_2 s} \\ &\quad + a_3(s)e^{-(\tau_1+\tau_2)s} = 0, \quad \tau_1,\tau_2 > 0 \end{aligned} \tag{2.5}$$

where $a_j(s),\ j = 0,1,2,3$ are polynomials of s with real coefficients while the highest degree of s in (2.5) only appears in $a_0(s)$, rendering (2.5) a "retarded system" [31]. The last term in (2.5) is the "cross-talk" between the two delays.

In order to get the stability charts for the given system, it is imperative to get the exhaustive sets of the imaginary roots, $s = \pm\omega_c i$, for the characteristic equation in (2.5) within the semi-infinite quadrant of $\tau_1, \tau_2 \in \Re^+$. Here, we follow the mathematical procedure described by [22] which evaluates the building curves. Accordingly, in (2.5), the exponential terms are replaced by:

$$e^{-\tau_k s} = \frac{1 - T_k s}{1 + T_k s}, \quad k = 1,2,\ T_k \in \Re \tag{2.6}$$

which is known as the Rekasius substitution [32] and is exact for $s = \pm\omega_c i$, $\omega \in \Re$ with the following relation between τ_k and T_k

$$\tau_k = \frac{2}{\omega}[\tan^{-1}(T_k\omega) \pm j\pi], \quad k = 1,2, \qquad j = 1,2,\ldots \tag{2.7}$$

The above equation describes an asymmetric mapping, in which one T is mapped into infinitely many $\tau's$ for a given $\omega \in \Re$. Inversely for the same ω, one particular τ corresponds to one T only. Rekasius substitution in (2.6) converts the infinite dimensional characteristic equation to a finite dimensional polynomial of ωi. In parallel, from (2.7) one can create the following relations for the SDS domain parameters (ν_1, ν_2)

$$T_k \omega = \tan(\frac{\nu_k}{2}) = z_k, \quad \nu_k = \tau_k \omega \in [0, 2\pi], \quad k = 1,2 \tag{2.8}$$

With the substitution of (2.6) and (2.8) in (2.5), one obtains a polynomial of ω with complex coefficients c_k which are parameterized in z_1, z_2

$$q(\omega, z_1, z_2) = \sum_{k=0}^{2} c_k(z_1, z_2)(\omega i)^k = 0 \tag{2.9}$$

If there is a solution $\omega \in \Re^+$ to (2.9), both its real and imaginary parts must be zero simultaneously:

$$\mathrm{Re}[q(\omega, z_1, z_2)] = \sum_{k=0}^{2} f_k(z_1, z_2)\omega^k = 0 \tag{2.10a}$$

$$\mathrm{Im}[q(\omega, z_1, z_2)] = \sum_{k=0}^{2} g_k(z_1, z_2)\omega^k = 0 \tag{2.10b}$$

In order for the equations (2.10a) and (2.10b) to have a common root, the following Sylvester's resultant matrix ought to be singular:

$$\mathbf{M} = \begin{bmatrix} f_2(z_1,z_2) & f_1(z_1,z_2) & f_0(z_1,z_2) & 0 \\ 0 & f_2(z_1,z_2) & f_1(z_1,z_2) & f_0(z_1,z_2) \\ g_2(z_1,z_2) & g_1(z_1,z_2) & g_0(z_1,z_2) & 0 \\ 0 & g_2(z_1,z_2) & g_1(z_1,z_2) & g_0(z_1,z_2) \end{bmatrix} \tag{2.11}$$

This results in the following expression in terms of z_1 and z_2:

$$\det(\mathbf{M}) = F(z_1, z_2) = F(\tan(\nu_1/2), \tan(\nu_2/2)) = 0 \tag{2.12}$$

which constitutes a closed form description of the kernel curves in the SDS $< \tau_1, \tau_2, \omega_c >$, i.e., the building curves. To obtain the SDS graphically, parameter v_2, can be scanned in the range of [0, 2π], so that the corresponding v_1 values can be calculated again in [0, 2π]. Notice that every point (ν_1, ν_2) on

these curves brings an imaginary characteristic root at $\pm\omega_c\, i$ which can be evaluated from (2.10a) or (2.10b), noting that they share the same $\pm\omega_c i$ root. Due to *Property 3*, namely the symmetricity property of building hypercurves, we keep in mind that both points $<\tau_1, \tau_2, \omega_c>$ and $<\tau_1, \tau_2, -\omega_c>$ are involved in SDS. Notice that we use $<\tau_1, \tau_2, \omega_c>$ values to obtain the TDS plot. Back transforming pointwise from the (ν_1, ν_2) domain of SDS to the (τ_1, τ_2) domain of delay space (DS), using the relation (2.7) with the appropriate positive ω values, one generates the kernel and offspring hypercurves.

The kernel and offspring curves divide the (τ_1, τ_2) domains in regions of possible stability and instability. To determine the stability nature of these regions we start from the non-delayed system (i.e., $\tau_1 = \tau_2 = 0$). We recite the definition of root tendency (RT).

Definition 3:Root Tendency (RT) The root tendency for each imaginary root $\omega_c i$, with respect to one of the time delays τ_1 or τ_2, is defined as

$$RT\Big|_{s=\omega_c i}^{\tau_j} = \operatorname{sgn}\left[\operatorname{Re}\left(S_{\tau_j}^{s}\Big|_{s=\omega_c i}\right)\right] \tag{2.13}$$

where $S_{\tau_j}^{s}\Big|_{s=\omega_c i} = \left.\dfrac{\partial s}{\partial \tau_j}\right|_{s=\omega_c i}$ is the sensitivity of the root with one of the delays fixed. ■

This property indicates the tendency of transition of the imaginary root, as the other delay increases. A slight different conceptualization of *RT* is defined within the SDS in the later segments of this chapter. The highlight of the discussion comes at making sense of transition properties in a domain (SDS) which is only defined pointwise.

2.2.3 Equivalency of Root Tendencies in SDS and DS Domains

In this section, the unexpected equivalency of the local stability transitions along the boundaries in SDS and DS is proven. For this, we follow two corresponding radial lines passing through the origin with a common slope in both spaces. This treatment can eliminate the influence of ω from DS to SDS. That is, if $\tau_2/\tau_1 = g,\ g \in \Re^+$, the radial lines in both domains are identical (i.e., $\tau_2\omega/\tau_1\omega = g,\ g \in \Re^+$). The corresponding points on them, however, are still earmarked by ω except the origin. Here, one may ask the following question: Departing from a certain delay composition that renders an imaginary characteristic root pair, if we increase the delays slightly along the mentioned radial line, how does the number of unstable roots (NU) change? We look at this question within both SDS and DS. As the main contribution of this chapter, we will prove that the local stability transition features within the SDS are identical to those within the DS. This discussion is obviously critical since it designates whether advancement along the radial line would have a stabilizing or destabilizing effect on the system. Before we introduce the main lemma, a new root tendency is defined.

Definition 4: Directional Root Tendency (DRT) The directional root tendency for each imaginary root $\omega_c i$, with respect to one of the time delays τ_1 or τ_2, is defined as

$$DRT\Big|_{\substack{s=\omega_c i \\ \tau_2=g\tau_1}}^{\tau_j} = \operatorname{sgn}\left[\operatorname{Re}\left(S_{\tau_1}^{s}\Big|_{\substack{s=\omega_c i \\ \tau_2=g\tau_1}}\right)\right] \tag{2.14}$$

where $S_{\tau_1}^{s}\Big|_{s=\omega_c i,\ \tau_2=g\tau_1} = (ds/d\tau_1)\Big|_{s=\omega_c i,\ \tau_2=g\tau_1}$ and $g \in \Re^+$ is the sensitivity of the root with one of the delays fixed. ■

This definition indicates the tendency of transition of the imaginary root, as the delays change along a radial line passing through the origin.

Lemma 1: Along the two corresponding radial lines (i.e., lines passing through the origin) with a common slope $g \in \Re^+$, one in the SDS and the other in the DS domain, the directional root tendencies of a purely imaginary roots remain identical.

Proof. A radial line is defined in SDS and DS as

$$\tau_2 = g\tau_1 \tag{2.15}$$

where $g \in \Re^+$ is the constant slope of the line. Substituting (2.15) into (2.5) yields

$$\begin{aligned} CE_{g,\tau}(s,\tau_1) = a_0(s) + a_1(s)e^{-\tau_1 s} + a_2(s)e^{-\tau_1 g s} \\ + a_3(s)e^{-(1+g)\tau_1 s} = 0, \quad \tau_1 > 0 \end{aligned} \tag{2.16}$$

which we name as directional characteristic equation. It is only valid on the line defined by (2.15) in both SDS and DS spaces. The DRT with respect to τ_1 along the radial line can be found by using (2.14). Taking the total derivative of (2.16) with respect to τ_1 yields

$$\frac{\partial CE_{g,\tau}}{\partial s}\frac{ds}{d\tau_1} + \frac{\partial CE_{g,\tau}}{\partial \tau_1} = 0 \tag{2.17}$$

$$S^{s}_{\tau_1}\Big|_{\substack{s=\omega_c \\ \tau_2 = g\tau_1}} = -\frac{\dfrac{\partial CE_{g,\tau}}{\partial \tau_1}}{\dfrac{\partial CE_{g,\tau}}{\partial s}} = s[H(s,\tau_1) - \tau_1]^{-1}\Big|_{\substack{s=\omega_c \\ \tau_2 = g\tau_1}} \tag{2.18}$$

where $H(s,\tau_1) = \dfrac{a_0' + a_1' e^{-\tau_1 s} + a_2' e^{-g\tau_1 s} + a_3' e^{-(1+g)\tau_1 s}}{a_1 e^{-\tau_1 s} + g a_2 e^{-g\tau_1 s} + (1+g)a_2 e^{-(1+g)\tau_1 s}}$ and $a_j' = da_j(s)/ds, j = 0,1,2,3$. The detailed derivation of (2.18) can be found in [33]. Then one can obtain

$$DRT\Big|^{\tau_1}_{\substack{s=\omega_c i \\ \tau_2 = g\tau_1}} = \operatorname{sgn}\left[\operatorname{Re}\left(S^{s}_{\tau_1}\Big|_{s=\omega_c i, \tau_2 = g\tau_1}\right)\right] = \operatorname{sgn}\left[\operatorname{Im}\left(H(s,\tau_1)\Big|_{s=\omega_c i, \tau_2 = g\tau_1}\right)\right] \tag{2.19}$$

The corresponding root sensitivity in SDS, however, does not exist in conventional sense. Because SDS is only meaningful at the stability transition boundaries and not in a continuum. Therefore, we wish to use the Rekasius substitution introduced in (2.6) which will provide a domain of continuum [29].

The substitution of (2.6) into Eq. (2.16) yields

$$CE_{g,T}(s,T_1)=a_0(s)+a_1(s)\frac{1-T_1s}{1+T_1s}+a_2(s)\left(\frac{1-T_1s}{1+T_1s}\right)^g+a_3(s)\left(\frac{1-T_1s}{1+T_1s}\right)^{g+1}=0 \tag{2.20}$$

The complete set of imaginary roots $s=\omega i,\omega\in\Re$ of the characteristic equations in (2.20) and (2.16) coincide, although the other roots have no correspondence. This feature suggests that one can use (2.20) instead of (2.16) to determine the imaginary roots $s=\omega i,\omega\in\Re$.

The relation (2.8) clearly represents corresponding monotonous relation between the variations of ν_j and T_j. Therefore the DRT in SDS along the $\tau_2\omega/\tau_1\omega=g$ radial line could be determined using the derivatives with respect to the only remaining parameter in (2.20), T_1.

The DRT with respect to T_1 along the radial line of slope g, can be found by using Definition 4. The total derivative of (2.20) with respect to T_1 is

$$\frac{\partial CE_{g,T}}{\partial s}\frac{ds}{dT_1}+\frac{\partial CE_{g,T}}{\partial T_1}=0 \tag{2.21}$$

which results in:

$$S^{s}_{T_1}\Big|_{\substack{s=\omega_c i\\ \tau_2=g\tau_1}}=\left.\frac{ds}{dT_1}\right|_{\substack{s=\omega_c i\\ \tau_2=g\tau_1}}=-\frac{\partial CE_{g,T}}{\partial T_1}\Big/\frac{\partial CE_{g,T}}{\partial s}=s[P(s,T_1)-T_1]^{-1}\Big|_{\substack{s=\omega_c i\\ \tau_2=g\tau_1}} \tag{2.22}$$

where $P(s,T_1)=\dfrac{a_0'+a_1'\frac{1-T_1s}{1+T_1s}+a_2'(\frac{1-T_1s}{1+T_1s})^g+a_3'(\frac{1-T_1s}{1+T_1s})^{1+g}}{[a_1\frac{1-T_1s}{1+T_1s}+ga_2(\frac{1-T_1s}{1+T_1s})^g+(1+g)a_2(\frac{1-T_1s}{1+T_1s})^{1+g}]\Big/2(1-T_1s)(1+T_1s)}$

and $a_j'=da_j(s)/ds,\ j=0,1,2,3$. The detailed derivation of (2.22) is left to [33]. Simplifying $P(s,T_1)$ using the properties of (2.6), (2.22) can be reduced to a similar expression as (2.18):

$$\left.\frac{ds}{dT_1}\right|_{\substack{s=\omega_c i\\ \tau_1=g\tau_2}} = s[\frac{H(s,\tau_1)}{m} - T_1]^{-1}\Big|_{s=\omega_c} \tag{2.23}$$

where $m = 2[(1-T_1 s)(1+T_1 s)]^{-1}$ for $s = \omega_c i$ and $H(s,\tau_1)$ is defined in (2.18). Using (2.23) in (2.14) for the DRT with respect to T, one obtains

$$DRT\Big|^{T_1}_{\substack{s=\omega_c i\\ \tau_2=g\tau_1}} = \text{sgn}\left[\text{Re}\left(S^{s}_{T_1}\Big|_{s=\omega_c i,\tau_2=g\tau_1}\right)\right] = \text{sgn}\left[\text{Im}\left(H(s,\tau_1)\Big|_{s=\omega_c i,\tau_2=g\tau_1}\right)\right] \tag{2.24}$$

which declares $DRT\Big|^{T_1}_{s=\omega_c i,\tau_2=g\tau_1} = DRT\Big|^{\tau_1}_{s=\omega_c i,\tau_2=g\tau_1}$. Therefore, we conclude

$$DRT\Big|^{\tau_1}_{s=\omega_c i,\tau_2=g\tau_1} = DRT\Big|^{T_1}_{s=\omega_c i,\tau_2=g\tau_1} = DRT\Big|^{v_1}_{s=\omega_c i,\tau_2=g\tau_1} \tag{2.25}$$

with only one constraint as given in (2.15). That is the DRT's are identical between SDS and DS so long as the variations are along the radial line segments. ♦

Remark 1: According to the continuity argument [27], given any point $(\tau_1^0, \tau_2^0) \in \Re^{2+}$ in the domain of the delays, we can calculate *NU* of (2.5) on the right half of the complex plane following the procedure below:

(a) Find the *NU* of Eq. (1) for the delay-free case when $(\tau_1, \tau_2) = (0,0)$;

(b) Generate the building and reflection hypercurves $\wp_0^{SDS} \cup \wp^{SDS}$ in SDS and the corresponding kernel and offspring hypercurves $\wp_0^{DS} \cup \wp^{DS}$ in DS;

(c) Draw two corresponding radial lines with a common slope $g = \frac{\tau_2^0}{\tau_1^0}$, one in SDS and the other in DS; Then find the intersection points of $\wp_0^{DS} \cup \wp^{DS}$ and the radial line, i.e., $\left\{(\tau_1^i, \tau_2^i) \in DS\right\}\Big|_{i=1}^{N}$

between origin and (τ_1^0, τ_2^0) in DS and locate the corresponding points $\left\{(\tau_1^i\omega_i, \tau_2^i\omega_i) \in SDS\right\}\Big|_{i=1}^{N}$ in SDS;

(d) Calculate the DRT's of each point in $\left\{(\tau_1^i\omega_i, \tau_2^i\omega_i) \in SDS\right\}\Big|_{i=1}^{N}$ and use that information (as per Lemma 1) to find *NU* for the point $(\tau_1^0, \tau_2^0) \in \Re^{2+}$ in DS.

2.2.4 Illustrative Example

In this subsection, an example case study is presented to illustrate the features mentioned above. For this, we take the characteristic equation (2.5) as

$$CE_\tau(s, \tau_1, \tau_2) = s^2 + 7.1s + 21.1425 + (6s + 14.8)e^{-\tau_1 s} + (2s + 7.3)e^{-\tau_2 s} + 8e^{-(\tau_1+\tau_2)s} = 0 \tag{2.26}$$

By using the substitutions (2.6) and (2.8), the characteristic equation (2.26) can be rewritten as

$$\begin{aligned} q(\omega, z_1, z_2) = {} & (-z_1 i - z_2 i + z_1 z_2 - 1)\omega^2 + (-3.1z_1 - 11.1z_2 + 0.9z_1 z_2 i + 15.1i)\omega \\ & + 5.6425z_1 i + 20.635z_2 i - 7.0425z_1 z_2 + 51.2425 \end{aligned} \tag{2.27}$$

If there is a solution $\omega \in \Re^+$ to (2.27), then both the real and imaginary parts must be zero at the same time, that is

$$\mathrm{Re}\left[q(\omega, z_1, z_2)\right] = (z_1 z_2 - 1)\omega^2 + (-3.1z_1 - 11.1z_2)\omega - 7.0425z_1 z_2 + 51.2425 \tag{2.28}$$

$$\mathrm{Im}\left[q(\omega, z_1, z_2)\right] = (-z_1 - z_2)\omega^2 + (0.9z_1 z_2 + 15.1)\omega + 5.6425z_1 + 20.6425z_2 \tag{2.29}$$

In order for (2.28) and (2.29) to have a common root, the Sylvester resultant matrix **M** should be singular

$$\mathbf{M} = \begin{bmatrix} z_1 z_2 - 1 & -3.1z_1 - 11.1z_2 & 51.2425 - 7.0425z_1 z_2 & 0 \\ 0 & z_1 z_2 - 1 & -3.1z_1 - 11.1z_2 & 51.2425 - 7.0425z_1 z_2 \\ -z_1 - z_2 & 0.9z_1 z_2 - 15.1 & 5.6425z_1 + 20.6425z_2 & 0 \\ 0 & -z_1 - z_2 & 0.9z_1 z_2 - 15.1 & 5.6425z_1 + 20.6425z_2 \end{bmatrix} \tag{2.30}$$

Therefore, the following equation should hold

$$
\begin{aligned}
\det(\mathbf{M}) = F(z_1, z_2) = F(\tan(v_1/2), \tan(v_2/2)) = \\
&- \tan(v_1/2)^4 \left[5.70 \tan(v_2/2)^4 - 37.35 \tan(v_2/2)^2 + 54.22\right] \\
&- \tan(v_1/2)^3 \left[-21.68 \tan(v_2/2)^3 + 333.52 \tan(v_2/2)\right] \\
&+ \tan(v_1/2)^2 \left[461.53 \tan(v_2/2)^4 + 1042.27 \tan(v_2/2)^2 - 583.43\right] \\
&+ \tan(v_1/2)\left[95.28 \tan(v_2/2)^3 + 1788.08 \tan(v_2/2)\right] \\
&- 2543.36 \tan(v_2/2)^4 - 11112.28 \tan(v_2/2)^2 - 11683.80 = 0
\end{aligned}
\tag{2.31}
$$

This expression is the description of the kernel hypercurves in the Spectral Delay Space (SDS), namely the building curves. By scanning v_2 in the range of [0, 2π], corresponding v_1 values are found. By using the Property 3, the Building Block (BB) is obtained. Then stacking the copies of the BB, the reflection curves are drawn. The SDS plot is available in Fig. 1. In order to plot the kernel and offspring curves, the common imaginary characteristic root $\pm\omega i$ for each set of (v_1, v_2) is found by using either (2.28) or (2.29). Then, the (v_1, v_2) domain of SDS is back transformed to the (τ_1, τ_2) delay space by using the corresponding ω values, and the kernel and offspring curves in (τ_1, τ_2) delay space are plotted in Fig. 2.

In Fig. 1, the blue curves represent (v_1, v_2, ω) sets with both positive and negative ω values. Since the (τ_1, τ_2) delay space is obtained from the (v_1, v_2, ω) sets with positive ω values, the intersections of the radial line and the positive ω curves are the ones that we are interested in. The lines in black in both figures represent $g = 0.89$ lines. The green points named as $B_k, k = 1,\ldots 6$ are the intersection points of $g = 0.89$ line and building – reflection curves in Fig. 1, where they are the intersection points of $g = 0.89$ line and kernel – offspring curves in Fig. 2.

After the set of $(T_1.T_2)$ for each set of (v_1, v_2, ω) is found for each point $B_k, k = 1,\ldots 6$, we have all the $\tau_1, \tau_2, \omega, v_1, v_2, T_1, T_2$ values at hand. Then, $RT\big|_{s=\omega_c i}^{\tau}$ and $RT\big|_{s=\omega_c i}^{T}$ can be verified according to Definition 3.

Table 1. The τ_1, τ_2, ω, v_1, v_2, T_1, T_2, $RT|_{s=\omega i}^{\tau_1}$, $RT|_{s=\omega i}^{T_1}$ values for each intersection point B_k, $k=1,...,6$.

	B1	B2	B3	B4	B5	B6
τ_1	0.39	1.91	1.59	5.26	3.63	6.17
τ_2	0.44	2.15	1.79	5.91	4.08	6.94
ω	6.12	1.72	5.44	1.79	4.18	2.51
v_1	2.38	3.29	8.67	9.43	15.16	15.50
v_2	2.67	3.70	9.74	10.60	17.02	17.42
T_1	0.41	-7.61	0.47	-242.0	0.84	3.79
T_2	0.68	-2.02	-1.16	-0.84	-0.31	-0.34
$RT\|_{s=\omega i}^{\tau_1}$	1	-1	1	-1	1	-1
$RT\|_{s=\omega i}^{T_1}$	1	-1	1	-1	1	-1

As shown in Table 1, the $\tau_1, \tau_2, \omega, v_1, v_2, T_1, T_2$, $RT\Big|_{s=\omega_c i}^{\tau}$, $RT\Big|_{s=\omega_c i}^{T}$ values for each point $B_k, k=1,...6$ are listed. As seen in the Table 1, for each intersection point, root tendencies with respect to τ_1 and T_1 are equal. For each intersection point $B_k, k=1,...6$, each v_j and T_j, where $j=1,2$ are monotonous for constant ω value. As a result, we can predict the stability transitions through these points while walking along the $g=0.89$ radial line in SDS, without going to TDS.

It is important to point out that all the intersection points should be found in the SDS, so that root tendencies can be found for each point. Those intersection points repeat themselves as $(v_1, v_2) \to (\infty, \infty)$;

however, to detect the locations of all the intersection points, the initial intersection points for all the repeating sets should be found. Then, the local stability transitions can be found without going to TDS.

2.3 Frequency Sweeping Method for Kernel and Offspring Hypercurves

2.3.1 Introduction

Frequency sweeping method is another way to determine Kernel and Offspring hypersurfaces (KOH) in the domain of the delays. It is widely known that for MTDS with $l > 3$, the calculation of the KOH in the p-dimensional (p-D) delay space is known to be computationally infeasible [34]. Instead, we examine its intersection with a 2-D space of two arbitrarily selected delays. For this, we deploy a frequency sweeping technique which is completely numerical [35]. This technique sweeps the only parameter, the frequency. Thus it is considered to be more effective for systems with higher orders and multiple delays than those techniques that require symbolic computations [36]. We will show that for this frequency sweeping technique, the knowledge of the exact upper and lower bounds of the imaginary spectra are needed. These bounds are known to exist for the retarded time delay system (1.2) [10]. To determine them, we adopt a half-angle tangent substitution method [37] and the Dixon resultant theory [38].

2.3.2 Preliminary: Half-angle Tangent Substitution

An LTI-MTDS in (1.2) is asymptotically stable if and only if all its characteristic roots are on the left half of the complex plane. The continuity of the characteristic roots of (2) with respect to the delays has

already been established in the literature [27]. Since the kernel and offspring hypercurves (KOH) are the only loci where characteristic equation (1.3) possesses imaginary roots, they are the only potential stability switching locations (thus often referred to as "stability switching" hypersurfaces). For a complete stability map one needs to determine all of these KOH exhaustively. The KH consists of points that exhibit the smallest positive delay values on all of the l delays. All OH are obtained from KH by a pointwise nonlinear transformation [29]. Thus, the mere knowledge of KH is sufficient to obtain the complete infinite set of OH. The determination of KH in l-D delay space is, however, computationally infeasible. We propose a simpler version of this general problem to "Determine the intersection of the kernel hypersurface on 2-D space of any two of the delays".

For the flow of the logic, readers who are not familiar with the CTCR paradigm are suggested to refer to the Appendix A for a brief review of the paradigm and its key propositions [29]. Here, we introduce a mathematical procedure called the "half-angle tangent substitution" that yields the determination of the complete cross-section of KH in the 2-D domain of the delays.

To determine $\mathbf{\Omega}$ on an arbitrarily-selected 2-D cross-section of the delay domain, for instance (τ_1, τ_2) without loss of generality, while all the remaining delays $\tau_3, \tau_4, ..., \tau_l$ are fixed we follow the steps below: For a root $s = \omega i$ we consider the Euler's formula for the transcendental terms in (1.3)

$$e^{-\tau_k s} = e^{-\tau_k \omega i} = \cos(\upsilon_k) - i\sin(\upsilon_k), \quad \upsilon_k = \tau_k \omega, \quad k = 1,2 \tag{2.32}$$

and express them in terms of a single parameter, the half-angle tangent:

$$\cos(\upsilon_k) = \frac{1 - z_k^2}{1 + z_k^2}, \quad \sin(\upsilon_k) = \frac{2z_k}{1 + z_k^2}, \quad z_k = \tan(\frac{\upsilon_k}{2}), \quad k = 1,2 \tag{2.33}$$

Notice that the inverse relation from z_k to τ_k is multi-valued as

$$\tau_k = \frac{2\tan^{-1}(z_k)}{\omega} + \frac{2r\pi}{\omega}, \quad 0 \le \tan^{-1}(.) < \pi, \quad k = 1,2, \quad r = 0,1,2,... \tag{2.34}$$

Substituting (2.33) into (1.3) again for an imaginary root $s = \omega i$, one obtains a new characteristic equation $\tilde{g}(s, \mathbf{z}, e^{-\tau_3 \omega i}, ..., e^{-\tau_l \omega i}) = 0$ where $\mathbf{z} = (z_1, z_2) \in \Re^2$. Following this domain transformation from $\boldsymbol{\tau}$ to $\{\mathbf{z}, \tau_3, \tau_4, ...\}$ and multiplying with the least common multiple of the denominators of $\tilde{g}$ we obtain a modified characteristic equation as

$$\bar{g}(s, \mathbf{z}, e^{-\tau_3 \omega i}, ..., e^{-\tau_l \omega i}) = \tilde{g}(s, \mathbf{z}, e^{-\tau_3 \omega i}, ..., e^{-\tau_l \omega i}) \prod_{k=1}^{2} (1 + z_k^2)^{c_k} = 0 \tag{2.35}$$

where $c_k = rank(\mathbf{B}_k) \le n$ is the commensurate degree of τ_k. This operation further simplifies the problem of determining the complete set of imaginary roots of (2.35) in the space of $\mathbf{z} \in \Re^2$ as described next.

2.3.3 Main Result

In order to extract the 2-D cross-section in (τ_1, τ_2) domain of the l-D KH, we fix all the remaining delays $\tau_3, \tau_4, ..., \tau_l$, without loss of generality. Suppressing these fixed delays in the arguments, the characteristic equation is renamed as

$$\hat{g}(\omega i, z_1, z_2) = \bar{g}(s, \mathbf{z}, e^{-\tau_3 \omega i}, ..., e^{-\tau_p \omega i}) = 0 \tag{2.36}$$

We denote the complete set of the *imaginary* eigenvalues of the system (2.36) as $\overline{\boldsymbol{\Omega}}$. It is apparent that $\overline{\boldsymbol{\Omega}} \subset \boldsymbol{\Omega}$. To determine $\overline{\boldsymbol{\Omega}}$, we deploy the half angle tangent substitution above and the Dixon resultant theory [38] as explained below. If there is a solution $\omega \in \Re^+$ in (2.36), it should make both the real and imaginary parts of this equation zero simultaneously

$$\mathrm{Re}[\hat{g}(\omega i, z_1, z_2)] = \sum_{j=0}^{2c_2} a_j(\omega, z_1) z_2^j = 0 \tag{2.37}$$

$$\mathrm{Im}[\hat{g}(\omega i, z_1, z_2)] = \sum_{j=0}^{2c_2} b_j(\omega, z_1) z_2^j = 0 \tag{2.38}$$

where the coefficients $a_j's$ and $b_j's$ are polynomials in z_1. They have real coefficients which are transcendental functions of ω. As a practical procedure, we deploy the Dixon resultant methodology of [39, 40] to create the necessary and sufficient conditions for the common root $\omega \in \Re^+$ of (2.37) and (2.38).

A. Dixon Resultant Concept and Discriminant for Polynomials

The Dixon resultant method has been widely used to solve the necessary and sufficient conditions for a set of polynomial equations to possess nontrivial common solutions [39]. It is one of many peer methodologies, such as Sylvester [41], Macaulay [42] and sparse [43] resultant formulations. In this chapter, we deploy the Dixon resultant, due to its computational efficiency over the others [44] on the two polynomials of interest, (2.37) and (2.38).

We present an overview of the key characteristics of the Dixon resultant theory following [40]. For notational simplicity, we denote the polynomials in (2.37) and (2.38) for fixed values of ω and z_1 as

$$p_1(z_2) \equiv \text{Re}[\hat{g}(\omega i, z_1, z_2)] \tag{2.39}$$

$$p_2(z_2) \equiv \text{Im}[\hat{g}(\omega i, z_1, z_2)] \tag{2.40}$$

The Dixon resultant is formulated to provide the necessary and sufficient condition for a common z_2 solution between the equations (2.37) and (2.38). Next consider the following polynomial in z_2

$$\delta(z_2, \alpha) = \frac{1}{(z_2 - \alpha)} \begin{vmatrix} p_1(z_2) & p_2(z_2) \\ p_1(\alpha) & p_2(\alpha) \end{vmatrix} \tag{2.41}$$

where $p_i(\alpha), i = 1, 2$ stands for replacing z_2 by α which is a new variable. The polynomial δ is known as the **Dixon polynomial**. It is symmetric with respect to α and z_2. The reason for symmetry is clear from (2.41) that when the arguments α and z_2 are exchanged, the expression remains invariant, i.e.,

$\delta(\alpha, z_2) = \delta(z_2, \alpha)$. Furthermore δ is of degree $d_{\max} - 1$ in α where $d_{\max} = \max[\deg(p_1, z_2), \deg(p_2, z_2)]$ and the notation $\deg(p_1, z_2)$ is used to represent the maximum degree of z_2 terms in the polynomial p_1. Since each common zero of p_1 and p_2 is a zero of $\delta(z_2, \alpha)$ regardless of α values, the coefficient of each power product of α in $\delta(z_2, \alpha)$ must be zero at this common zero of p_1 and p_2. This results in $d_{\max}$ equations corresponding to these coefficients (which are polynomials in z_2) of α^i $(i = 0,1,...,d_{\max} - 1)$. The coefficient matrix $\mathbf{F}(\omega, z_1) \in \Re^{d_{\max} \times d_{\max}}$ of these $d_{\max}$ equations is known as the **Dixon matrix**

$$\mathbf{F}(\omega, z_1) \begin{pmatrix} 1 \\ z_2 \\ \vdots \\ z_2^{d_{\max}-1} \end{pmatrix} = \begin{pmatrix} 0 \\ 0 \\ \vdots \\ 0 \end{pmatrix} \tag{2.42}$$

For a nontrivial solution of (2.42), $\mathbf{F}(\omega, z_1)$ should be singular [40]

$$\det\left[\mathbf{F}(\omega, z_1)\right] = 0 \tag{2.43}$$

This gives the necessary and sufficient condition on the coefficients of p_1 and p_2 in terms of the fixed ω and z_1 for a common z_2 solution of (2.37) and (2.38). The multinomial expansion of the determinant in (2.43) is known to be the Dixon Resultant [39]. We denote it as $Rz_2(\omega, z_1) = \det\left[\mathbf{F}(\omega, z_1)\right]$. Similarly the notation Rz_2 would represent the "Resultant" based on z_2.We wish to formalize this development by the following theorem, proof of which follows the above explanations.

Theorem 1 ([45]): The necessary and sufficient condition for two polynomials $p_1(z_2)$ and $p_2(z_2)$ to have a nontrivial common zero is that the corresponding **Dixon matrix** $\mathbf{F}(\omega, z_1)$ is singular, i.e.

$$Rz_2(\omega, z_1) = \det\left[\mathbf{F}(\omega, z_1)\right] = 0 \tag{2.44}$$

Consequently, if the boundaries of ω is known one can sweep it in this interval and obtain the corresponding $z_1 \in \Re$ values from $Rz_2 = 0$. Furthermore, with the knowledge of ω and $z_1 \in \Re$, the

corresponding $z_2 \in \Re$ values are obtained from (2.37) or (2.38). For increased efficiency of this process the deterministic knowledge of ω bounds would be very helpful. The main contribution of this subsection appears at this venue. The procedure to achieve this is described below in several steps.

(i) We first establish the continuity and differentiability of ω with respect to z_1 (or z_2). The detailed proofs are elaborated in the following subsection B.

(ii) Next, for the minimum and maximum values of ω we explore the extremum condition of $\partial\omega/\partial z_1 = 0$ (or $\partial\omega/\partial z_2 = 0$). Combining this with (2.44), we search for the common roots of $Rz_2 = 0$ (2.44) and $\partial\omega/\partial z_1 = 0$. These two equations, in fact, lead to $\frac{\partial Rz_2}{\partial z_1} + \frac{\partial Rz_2}{\partial \omega}\frac{\partial \omega}{\partial z_1} = 0$ and

$$\partial Rz_2 / \partial z_1 = 0 \tag{2.45}$$

The conditions (2.44) and (2.45) together define the Discriminant [38]. A formal definition is presented next.

Definition 5 [38] : Discriminant of Rz_2**:** The discriminant of Rz_2 with respect to z_1, denoted by $Dz_1(\omega)$, is the resultant formed using the two polynomials Rz_2 and $\partial Rz_2 / \partial z_1$ by eliminating z_1. ■

This operation, in fact, is the same Dixon procedure as above but this time to guarantee the common roots of (2.44) and (2.45). Note that $Dz_1(\omega)$ is a function of only one argument, ω, and by solving its roots and eliminating the complex ones we can obtain the upper and lower bounds of ω. A formal description of this procedure is given as a theorem in the following subsection C.

B. Differentiability of ω with Respect to z_i

As a preparatory step to the main theorem in the next subsection, we prove the continuity and differentiability of ω with respect to z_i. For this, we use the *Rekasius substitution [32]*

$$e^{-\tau_i s} = \frac{1-T_i s}{1+T_i s}, \quad T_i \in \Re,\ i = 1,2,...,l \tag{2.46}$$

where $T_i \in \Re$ is the agent parameter. This is an exact substitution when $s = \omega i, \omega \in \Re^+$ with the following relation between τ_i and T_i:

$$\tau_i = \frac{2}{\omega}[\tan^{-1}(T_i\omega) \pm j\pi], \quad i = 1,2,...,l, \qquad j = 0,1,2,... \tag{2.47}$$

The substitution of (2.46) into (1.3) yields a new characteristic equation $f_T(s,\mathbf{T}) = 0$, where $\mathbf{T} = (T_1, T_2, ..., T_l) \in \Re^l$. Further manipulated form of this equation is

$$\hat{f}_T(s,\mathbf{T}) = f_T(s,\mathbf{T})\prod_{i=1}^{l}(1+T_i s)^{c_i} = \sum_{i=0}^{m} a_i(\mathbf{T})s^i = 0 \tag{2.48}$$

where $a_i's$ are multinomials in $\mathbf{T}$, $c_i = rank(B_i) \le n$ is the commensurate degree for τ_i and $m = n + \sum_{i=1}^{l} c_i \le (l+1)n$. It is very critical to recite the proven feature that only the imaginary spectra of (2.48) are identical to that of (1.3) while the remaining finite spectra of (2.48) and infinite spectra of (1.3) have no correspondence. To determine the imaginary spectra of (2.48), we deploy the parametric Routh's array with the agent parameter $\mathbf{T}$ as it is done in [46].

Table 2. Routh's array for $\hat{f}_T(s,\mathbf{T})$

s^m	$a_m(\mathbf{T})$	$a_{m-2}(\mathbf{T})$	...	a_0
s^{m-1}	$a_{m-1}(\mathbf{T})$	$a_{m-3}(\mathbf{T})$	...	
$\vdots$	$\vdots$	$\vdots$	$\vdots$	
s^4	$R_{41}(\mathbf{T})$	$R_{42}(\mathbf{T})$	$R_{43}=a_0$	
s^3	$R_{31}(\mathbf{T})$	$R_{32}(\mathbf{T})$		
s^2	$R_{21}(\mathbf{T})$	$R_{22}=a_0$		
s^1	$R_1(\mathbf{T})$			
s^0	$R_0=a_0$			

Remark 2: According to [47, pg 398], we assume that $a_0 \neq 0$ in the Routh's array of Table 2. This assumption is to assure that any zero root of $\hat{f}_T(s,\mathbf{T})=0$ is removed before we continue further.

Lemma 2: In a Routh's array such as Table 2, the parametric setting $\mathbf{T}_0=(T_{10},T_{20},...,T_{l0})\in\Re^l$ which makes both $R_1(\mathbf{T})=0$ and $R_{21}(\mathbf{T})=0$, also makes $R_{31}(\mathbf{T}_0)=0$ and $R_{32}(\mathbf{T}_0)=0$. This implies that at such a point the dynamics which is represented by this array always possesses two pairs of symmetric roots with respect to the origin [47].

Proof: From the Routh's array formation, one has

$$R_1(\mathbf{T}_0)=\frac{R_{21}(\mathbf{T}_0)R_{32}(\mathbf{T}_0)-R_{31}(\mathbf{T}_0)a_0}{R_{21}(\mathbf{T}_0)}=0 \tag{2.49}$$

where a_0 is assumed to be non-zero according to Remark 2. Since $R_{21}(\mathbf{T}_0)=0$, we have $R_{31}(\mathbf{T}_0)=0$, otherwise $R_1(\mathbf{T}_0)=0$ becomes infinity. In addition,

$$R_{21}(\mathbf{T}_0)=\frac{R_{31}(\mathbf{T}_0)R_{42}(\mathbf{T}_0)-R_{32}(\mathbf{T}_0)R_{41}(\mathbf{T}_0)}{R_{31}(\mathbf{T}_0)}=0 \tag{2.50}$$

Upon substitution of (2.50) into (2.49), the expression $R_1(\mathbf{T}_0)$ transforms to:

$$R_1(\mathbf{T}_0) = \frac{[R_{31}(\mathbf{T}_0)R_{42}(\mathbf{T}_0) - R_{32}(\mathbf{T}_0)R_{41}(\mathbf{T}_0)]R_{32}(\mathbf{T}_0) - R_{31}^2(\mathbf{T}_0)a_0}{R_{31}(\mathbf{T}_0)R_{42}(\mathbf{T}_0) - R_{32}(\mathbf{T}_0)R_{41}(\mathbf{T}_0)} = 0 \tag{2.51}$$

Plugging $R_{31}(\mathbf{T}_0) = 0$ into (2.51), one obtains $R_1(\mathbf{T}_0) = R_{32}(\mathbf{T}_0) = 0$. Since both the terms in the s^3 row, i.e., $R_{31}(\mathbf{T}_0)$ and $R_{32}(\mathbf{T}_0)$, are zero, the auxiliary polynomial is formed from the coefficients of the s^4 row:

$$R_{41}(\mathbf{T}_0)s^4 + R_{42}(\mathbf{T}_0)s^2 + a_0 = 0 \tag{2.52}$$

From (2.52), one obtains two pairs of symmetric roots with respect to the origin, depending on the values of the coefficients the four roots may be real, imaginary or complex. ♦

Lemma 3: In the parametric domain $\mathbf{T} = (T_1, T_2, ..., T_l) \in \Re^l$, each branch of $R_1(\mathbf{T}) = 0$ that generates purely imaginary root $\omega \in \Re^+$ always remains inside the region where $R_{21}(\mathbf{T})R_{22}(\mathbf{T}) > 0$.

Proof: If the curve of $R_1(\mathbf{T}) = 0$ that generates nonzero purely imaginary root does not intersect with the curve $R_{21}(\mathbf{T})R_{22}(\mathbf{T}) = 0$, the lemma is trivially proven given the fact that $\omega \in \Re^+$ exists only when the conditions $R_1(\mathbf{T}) = 0$ and $R_{21}(\mathbf{T})R_{22}(\mathbf{T}) > 0$ hold simultaneously [29]. Thus, we assume that $R_1(\mathbf{T}) = 0$ intersects with $R_{21}(\mathbf{T})R_{22}(\mathbf{T}) = 0$ at $\mathbf{T}_0 = (T_{10}, T_{20}, ..., T_{l0}) \in \Re^l$ in the parametric domain $\mathbf{T}$. Since $R_{22}(\mathbf{T}) \equiv a_0$ is a non-zero constant term, it is clear that $R_1(\mathbf{T}) = 0$ intersects with $R_{21}(\mathbf{T}) = 0$ at $\mathbf{T}_0$. From Lemma 2, the intersection point of $R_1(\mathbf{T}) = 0$ and $R_{21}(\mathbf{T}) = 0$ makes both the numerator and denominator of $R_{21}(\mathbf{T})$ zero. Thus, the following three curves, i.e., $R_1(\mathbf{T})$, the numerator and the denominator of $R_{21}(\mathbf{T})R_{22}(\mathbf{T})$, intersect at a common point $\mathbf{T}_0$ in the parametric domain $\mathbf{T}$.

Next we prove by contradiction that marching across the intersection point $\mathbf{T}_0$ along $R_1(\mathbf{T}) = 0$ curve, the sign of $R_{21}(\mathbf{T})R_{22}(\mathbf{T})$ remains invariant. If this claim does not hold, then one pair of symmetric real roots

(corresponding to $R_{21}(\mathbf{T})R_{22}(\mathbf{T})<0$) changes to one pair of purely imaginary roots (corresponding to $R_{21}(\mathbf{T})R_{22}(\mathbf{T})>0$) or vice versa at an infinitesimal variation of vector $\mathbf{T}$. Thus $s=0$ has to be the transitioning root pair at $\mathbf{T}_0$ according to the root continuity argument. In addition, if at such a point $R_1(\mathbf{T}_0)=0$ and $R_{21}(\mathbf{T}_0)=0$, it yields $R_{31}(\mathbf{T}_0)=0$ and $R_{32}(\mathbf{T}_0)=0$ according to Lemma 2. Then the auxiliary polynomial is formed as shown in (2.52) with $s=0$ being a double root. Upon plugging $s=0$ into (2.52), one obtains $a_0=0$ and this contradicts the departing assumption in Remark 2. Therefore, marching across the intersection point $\mathbf{T}_0$ along $R_1(\mathbf{T})=0$ curve, the sign of $R_{21}(\mathbf{T})R_{22}(\mathbf{T})$ remains invariant. Furthermore, since $\omega\in\Re^+$ exists only when the condition $R_1(\mathbf{T})=0$ and $R_{21}(\mathbf{T})R_{22}(\mathbf{T})>0$ hold concurrently, Lemma 2 is proven. ♦

Theorem 2: The variations in the frequency of the purely imaginary root $\omega\in\Re^+$ of (2.36) is continuous and differentiable with respect to both variables $z_i=\tan(\tau_i\,\omega/2), i=1,2$.

Proof: We establish the root continuity and differentiability of $\omega\in\Re^+$ with respect to z_i through the intermediate agent parameter T_i used in the Rekasius substitution. For this, we assume that $\omega\in\Re^+$ is a function of $\mathbf{T}=(T_1,T_2,...,T_l)\in\Re^l$, i.e., $\omega\equiv\omega(\mathbf{T})$. The continuity and differentiability of $\omega\in\Re^+$ with respect to T_i $(i=1,2,...,l)$ are assured through Lemma 3. That is, $\partial\omega/\partial T_i$ exists for all $T_i\in[-\infty,\infty]$. From the definition of z_i and (2.7)

$$z_i=T_i\,\omega,\qquad i=1,2 \tag{2.53}$$

According to the chain rule,

$$\frac{\partial\omega}{\partial T_i}=\frac{\partial\omega}{\partial z_i}\frac{\partial z_i}{\partial T_i} \tag{2.54}$$

where $\partial z_i/\partial T_i=\omega+T_i\,\partial\omega/\partial T_i$ as per (2.53). Thus, one obtains

$$\frac{\partial \omega}{\partial z_i} = \frac{\partial \omega}{\partial T_i} \frac{1}{(\omega + T_i \, \partial \omega / \partial T_i)} \tag{2.55}$$

Since $\partial \omega / \partial T_i$ exists due to the earlier proven differentiability (2.55) implies that ω is differentiable with respect to z_i. Thus the continuity and differentiability of ω with respect to z_i $(i = 1,2)$ is established. ♦

C. Determination of the Bounds of the Imaginary Spectra

With the knowledge of Definition 5 and Theorem 2, we present the main theorem that reveals the exact upper and lower bounds of $\overline{\mathbf{\Omega}}$ for the case when the frequencies of the imaginary spectra are strictly positive, i.e., the lower bound is not zero.

Theorem 3: The exact positive upper and lower bounds of $\overline{\mathbf{\Omega}}$ are the maximum and minimum positive real roots of the discriminant of the resultant Rz_2, i.e., $Dz_1(\omega)$, which render $(z_1, z_2) \in \Re^2$ in (2.36).

Proof: For the extrema of ω, we expand $\partial \omega / \partial \tau_1$ using the chain rule as

$$\frac{\partial \omega}{\partial \tau_1} = \frac{\partial \omega}{\partial z_1} \frac{\partial z_1}{\partial \tau_1} = 0 \tag{2.56}$$

where $\partial z_1 / \partial \tau_1 = [1 + \tan^2(\upsilon_1 / 2)] \omega / 2$ according to (2.32) and (2.33). For all $\omega \in \Re^+$ this derivative is nonzero, thus we investigate the second term instead, i.e., $\partial \omega / \partial z_1 = 0$, in order to find the extrema of ω. In accordance with Theorem 2, we study the resultant $Rz_2 = 0$ and search for the conditions to enforce its real and imaginary parts to have a nontrivial common zero. Note that the differentiability of ω with respect to z_1 is proven in Theorem 2, therefore we the following can be written

$$\frac{\partial Rz_2}{\partial z_1} + \frac{\partial Rz_2}{\partial \omega} \frac{\partial \omega}{\partial z_1} = 0 \tag{2.57}$$

For the condition $\partial\omega / \partial z_1 = 0$ to hold, we must enforce $\partial Rz_2 / \partial z_1 = 0$. If these two equations $Rz_2 = 0$ and $\partial Rz_2 / \partial z_1 = 0$ held concurrently (2.37) and (2.38) will have a nontrivial common zero in ω which will also represent an extremum. This argument brings the concept of the discriminant of Rz_2, which is $Dz_1(\omega)$ in Definition 5. It is a function of ω only, zeros of which can be numerically determined. We denote all the positive real roots of this function as $\hat{\omega}_1, \hat{\omega}_2, ..., \hat{\omega}_{p-1}, \hat{\omega}_p$, p is a positive integer, with the relation $\hat{\omega}_1 < \hat{\omega}_2 < ... < \hat{\omega}_{p-1} < \hat{\omega}_p$. To calculate the upper bound of $\overline{\mathbf{\Omega}}$, we follow the steps below with the initial condition $i = l$ (i.e., the largest common frequency):

(a) Solve $Rz_2(\hat{\omega}_i, z_1) = 0$ for $z_1 \in \Re$. If no real solution exists, reduce i by 1 and repeat this step.

(b) For each $(\hat{\omega}_i, z_1) \in \Re^2$ composition obtained in (a), solve equation (2.37) or (2.38) for $z_2 \in \Re$. As per the necessary and sufficient condition of $Rz_2(\omega_i, z_1) = 0$ these roots should be common to both equations. Go to step (c). If there exists no common $z_2 \in \Re$ root for (2.37) and (2.38), then reduce i by 1 and return to (a).

(c) Check the value of i:

(c1) If $i > 1$, declare $\hat{\omega}_i$ as the upper bound of $\overline{\mathbf{\Omega}}$ and denote it with $\overline{\omega}$.

(c2) If $i = 1$ for such an upper bound, it would imply that the lower and upper bounds of the root crossing frequencies are identical. This is a rare and degenerate case. Following Lemma governs the stability outlook of this class of systems. ♦

Lemma 4: If the lower bound $\underline{\omega}$ and upper bound $\overline{\omega}$ of $\overline{\mathbf{\Omega}}$ are identical, it implies a delay independent stability behavior for the system (2.36) on $(\tau_1, \tau_2) \in \Re^{2+}$ space.

Proof: By following the construction steps of $\underline{\omega}$ and $\overline{\omega}$ above we already have a composition $(z_1, z_2) \in \Re^2$. We then solve for the corresponding τ_1 and τ_2 using (2.7), which declares the presence of a grid of infinitely many isolated points on the $(\tau_1, \tau_2) \in \Re^{2+}$ space with a grid size of $2\pi / \underline{\omega} = 2\pi / \overline{\omega}$. Keeping the root continuity rule in mind, we conclude that the roots approach to imaginary axis from either stable left half plane or unstable right half plane, but return without crossing over as the delay combination traverses through these isolated points. This conclusion is tantamount to declaring no change of stability throughout the $(\tau_1, \tau_2) \in \Re^{2+}$ space. That is, the case is delay independent stable or unstable. ♦

Excluding the above mentioned degenerate case, one can perform a similar procedure to determine the lower bound, $\underline{\omega}$, of $\overline{\mathbf{\Omega}}$ but this time starting from the initial condition of $i = 1$ and pursuing through the same steps as in (a, b, c) using an increasing counter i.

Remark 3: The lower bound $\underline{\omega}$ of $\overline{\mathbf{\Omega}}$ may be zero for a degenerate case. An example of such an exception is treated in [22] for the interested reader. Departing from the upper and lower bounds of $\overline{\mathbf{\Omega}}$, the following numerical procedures can be performed to get the 2-D cross-section of the l-D KOH.

(i) Sweep ω within the obtained bounds using an appropriate step size and solve $Rz_2(\omega, z_1) = 0$ for $z_1 \in \Re$ solution.

(ii) For each $(\omega, z_1) \in \Re^2$ composition obtained in (i), check if $z_2 \in \Re$ exists to satisfy (2.37) and (2.38) concurrently. If so, go to step (iii). Otherwise, return to (i) and scan the next ω value.

(iii) For the obtained $(\omega, z_1, z_2) \in \Re^3$ correspondences, back-construct the kernel delay composition $(\tau_1, \tau_2) \in \Re^{2+}$ as per (2.34) and the definition of KH.

The above procedure terminates when the entire interval of ω is swept. This process results in the 2-D intersection of the l-D KH in the $(\tau_1, \tau_2) \in \Re^{2+}$ space. Once they are found exhaustively, the steps of CTCR in Appendix A follow for the determination of the OH and the corresponding 2-D intersection of the stability map in $(\tau_1, \tau_2) \in \Re^{2+}$ space.

Remark 4: As stated earlier, Dixon resultant is computationally more efficient over the peer resultant formulations. Specifically, the preference of the Dixon resultant over the well-known Sylvester resultant is due to its faster computation speed for various practical cases [40]. One major reason for the computational efficiency is that Dixon resultant involves considerably less computation than Sylvester resultant does**.** It evaluates the determinant of a $\max(m,n) \times \max(m,n)$ -dimensional Dixon matrix **F** (where m and n are the degrees of z_2 in p_1 and p_2, respectively). This matrix is much smaller than the $(m+n) \times (m+n)$-dimensional Sylvester matrix.

2.3.4 Example Case Study

In order to demonstrate the capabilities of the proposed method, we take a system with $n = 2,\ p = 5$

$$\mathbf{A} = \begin{bmatrix} 0 & 3 \\ -24 & -9 \end{bmatrix}, \mathbf{B}_1 = \begin{bmatrix} -1 & 0.5 \\ -2 & -3 \end{bmatrix}, \mathbf{B}_2 = \begin{bmatrix} -2 & 0.1 \\ 1 & -1 \end{bmatrix}$$
$$\mathbf{B}_3 = \begin{bmatrix} 1 & 3 \\ -5 & 0.2 \end{bmatrix}, \mathbf{B}_4 = \begin{bmatrix} 2 & 0.5 \\ 1 & -1 \end{bmatrix}, \mathbf{B}_5 = \begin{bmatrix} 3 & 0 \\ -2 & 2 \end{bmatrix} \tag{2.58}$$

Notice that all $\mathbf{B}_i$ matrices have the rank 2, i.e., $c_i = 2,\ \ i = 1,2,...,5$. The characteristic equation of the system becomes

$$
\begin{aligned}
g(s,\boldsymbol{\tau}) = {} & s^2 + 9s + 72 + (4s+27)e^{-\tau_1 s} + (3s+17.4)e^{-\tau_2 s} + (-1.2s+78)e^{-\tau_3 s} - (s \\
& + 9)e^{-\tau_4 s} - (5s+21)e^{-\tau_5 s} + 4e^{-2\tau_1 s} + 1.9e^{-2\tau_2 s} + 15.2e^{-2\tau_3 s} - 2.5e^{-2\tau_4 s} + 6e^{-2\tau_5 s} \\
& + 6.7e^{-(\tau_1+\tau_2)s} + 5.3e^{-(\tau_1+\tau_3)s} - 4.5e^{-(\tau_1+\tau_4)s} - 10e^{-(\tau_1+\tau_5)s} - 3.9e^{-(\tau_2+\tau_3)s} - 0.6e^{-(\tau_2+\tau_4)s} \\
& - 6.8e^{-(\tau_2+\tau_5)s} - 1.1e^{-(\tau_3+\tau_4)s} + 8.6e^{-(\tau_3+\tau_5)s} + 2e^{-(\tau_4+\tau_5)s} = 0
\end{aligned}
\tag{2.59}
$$

In this equation, we arbitrarily fix $\tau_3 = 0.5$, $\tau_4 = 1.5$ and $\tau_5 = 1$. We suppress the steps involving the resultant and discriminant as in Definition 5, due to space constraints. According to Theorem 3, for this system and the three fixed delays the exact lower and upper bounds of the set $\overline{\boldsymbol{\Omega}}$ is determined to be $[3.8931, 13.3238]$. We next scan ω within this interval and apply the CTCR paradigm to reveal the stability map in (τ_1, τ_2) space as shown in Fig. 3. The red and blue curves are KH and OH, respectively.

In Fig.3, the RT invariance property is also marked at some selected points (0.31,0.04) to (1.40,0.04) and (0.23,0.38) to (0.75,0. 38). The deployment of CTCR starts with the determination of the stability at point $(\tau_1, \tau_2) = (0,0)$. For this, we follow two different procedures,

(i) The Quasi-Polynomial mapping-based Root-finder (QPmR) algorithm [20] which determines numerically the dominant characteristic root of a quasi-polynomial, s_{dom}, at a desirable precision. For $\tau_1 = 0$, $\tau_2 = 0$, $\tau_3 = 0.5$, $\tau_4 = 1.5$ and $\tau_5 = 1$, the real part of the dominant characteristic root of (2.59) is –0.62 and thus the system is stable at $(\tau_1, \tau_2) = (0,0)$ as shown in Fig.3.

(ii) CTCR paradigm. An alternative way to determine the stability of the system at $(\tau_1, \tau_2) = (0,0)$ is to apply the CTCR paradigm. Note that the delays are intentionally selected to have commensurate relations with each other as $\tau_3 = \tau$, $\tau_4 = 3\tau$ and $\tau_5 = 2\tau$, so that the system with $(\tau_1, \tau_2) = (0,0)$ is a simpler system with single but commensurate time delays in τ. Its characteristic equation is

$$g(s,\boldsymbol{\tau}) = s^2 + 16s + 129 + (-1.2s + 79.4)e^{-\tau s} - (5s + 22.6)e^{-2\tau s} - (s + 5.5)e^{-3\tau s} + 4.9e^{-4\tau s} + 2e^{-5\tau s} - 2.5e^{-6\tau s} = 0 \tag{2.60}$$

We then apply the Rekasius substitution (2.6) to (2.60) which converts it into a parameterized polynomial in s:

$$a_8(T)s^8 + a_7(T)s^7 + a_6(T)s^6 + a_5(T)s^5 + a_4(T)s^4 + a_3(T)s^3 + a_2(T)s^2 + a_1(T)s^1 + a_0(T) = 0 \tag{2.61}$$

where

$a_8(T) = 10T^6$; $a_7(T) = 132T^6 + 60T^5$; $a_6(T) = 329T^6 + 908T^5 + 150T^4$;

$a_5(T) = 4244T^5 + 2480T^4 + 200T^3$; $a_4(T) = 14917T^4 + 3400T^3 + 150T^2$;

$a_3(T) = 27400T^3 + 2420T^2 + 60T$; $a_2(T) = 23387T^2 + 812T + 10$;

$a_1(T) = 10436T + 88$; $a_0(T) = 1847$.

This equation shares identical imaginary roots with (2.60). To determine the imaginary spectra of (2.61), we deploy the Routh's array. If there is a pair of imaginary roots of (2.61), the only term on the row corresponding to s^1, i.e. , $R_1(T)$, must be zero for a $T \in \Re$ to generate possible stability switching points in τ. The Routh's array yields the $R_1(T)$ term for (2.61) as

$$R_1(T) = 2.0026\ 10^{12}T^{12} + 1.8894\ 10^{12}T^{11} + 9.3655\ 10^{11}T^{10} + 2.6274\ 10^{11}T^9 + 5.3566\ 10^{10}T^8 + 9.0511\ 10^9T^7 + 1.1037\ 10^9T^6 + 87978715.0227T^5 + 4944962.5095T^4 + 206443.7782T^3 + 5909.6454T^2 + 102.8591T + 1 = 0 \tag{2.62}$$

Note that all the numerical values in (2.62) are truncated to conserve space. All twelve roots of (2.62) are complex numbers. That means the system (2.60) does not offer any imaginary root crossing for any $T \in \Re$ or any τ. That is, its stability remains the same as that of the non-delayed system. It is trivial to check that (2.60) is stable when $\tau = 0$ and hence it remains stable for all τ values, specifically for $\tau = 0.5$ which corresponds to the delay values of interest $\tau_3 = 0.5$, $\tau_4 = 1.5$ and $\tau_5 = 1$. This yields

the same stability declaration for the system which was obtained using the QPmR algorithm (mentioned earlier in this section).

Once the stability nature of $(\tau_1, \tau_2) = (0,0)$ point is determined we progress further determining the NU values at various partitions of the delay space as displayed sparsely in Fig. 3, shaded regions are the stable regions with NU=0.

3. Novel and Paradoxical Philosophies: Sign Inverting Control and Delay Scheduling Control Schemes

3.1 Description

This thesis focuses on the control synthesis for linear time-invariant time delayed systems. Such studies resulted in the development of several concepts including *Delay Scheduling Control* (*DSC*) and *Sign Inverting Control* (*SIC*). Earlier development of DSC is discussed in several publications leading to [23] which handle multiple-delay cases with experimental validations. The article [24], on the other hand, is the only archival document on SIC. It presents the preliminary development on the concept which treats the class of dynamics with a single delay only. The present thesis is prepared with two additional contributions in mind:

(i) It is the first treatise of SIC under multiple independent and large delays;

(ii) It is the only attempt on the combination of SIC and DSC techniques.

For SIC, we explore how the change in polarity of the delayed states influences the delay-dependent stability characteristics of (1.2). Let us define an *inverted* system in this context, which is described by

$$\dot{\mathbf{x}} = \mathbf{A}\mathbf{x} - \sum_{i=1}^{l} \mathbf{B}_i \mathbf{x}(t-\tau_i) \tag{3.1}$$

Compared to the *original* system (1.2), the polarity of all delayed terms contained in the dynamics is effectively inverted by the sign change in all $\mathbf{B}_i$. The characteristic equation for this configuration becomes

$$\overline{CE}(s,\boldsymbol{\tau}) = \det(s\mathbf{I} - \mathbf{A} + \sum_{i=1}^{l} \mathbf{B}_i e^{-\tau_i s}) \tag{3.2}$$

The infinite-dimensional systems in (1.2) and (3.1) are declared globally asymptotically stable if their respective characteristic equations (1.3) and (3.2) have all their spectra on the left-half of the complex plane. It is trivial to claim that the infinite spectra of (1.3) and (3.2) are completely different. Their respective imaginary spectra, however, show some intriguing correspondence to each other, and we focus on these features, as shown in the following subsections.

We wish to emphasize that for both SIC and DSC operations, as well as for the stability paradigm CTCR, an important attribute is the "large delays". By "large" we mean that the delays encountered in the operation are in the order of magnitude of the period of the fastest controlled dynamics. Say, for a desired trajectory which has 10 Hz as the highest frequency content, this study is focusing on control feedback delays in the order of 10^{-1} second (sec). The practical implication of this point is that small delays (such as a few-sampling periods) are not of concern. On the contrary, this line of study investigates cases which bring much longer sensing and actuation delays, which are characterized as "feedback delays".

Sign Inverting Control idea originates from a very favorable but practical suggestion: in SIC the controller inverts the polarity of the "original" control actuation (e.g., a servo motor receiving a –V input voltage instead of +V). This action is based on the expectation that stable operating regions of a TDS may be expanded considerably by simply reversing the sign of the feedback gains. The mathematical implication of this concept is more intriguing, as we will describe in the later sections of the thesis. If the resulting stability maps for both original and SIC strategies are known crisply, the control designer will have much larger choice of delay selections to make without jeopardizing stability. In other words, by inverting the sign of the feedback control, stronger delay robustness may be achieved. The selection rules of the control strategy for different delay compositions are the main questions we attempt to answer in this Section. We present several angles of approach within the text to resolve this nontrivial problem.

Delay Scheduling Control is another control concept which is based on deliberately increasing delays such that control performance is improved [23]. The highlight of this paradoxical scheme is to schedule the delays by *prolonging* them further. This is a counter-intuitive proposition but it is the only game we can impose on delays. They cannot be reduced beyond what they are at the present, due to causality of the dynamic events; however, they can be prolonged further by the controller. For instance, additional "hold buffers" can be artificially introduced in the feedback line of the controlled system. Owing to the complex infinite dimensionality of the delayed dynamics such manipulations on the delays may create some improved characteristics also. For instance, disturbance rejection speeds may be improved by these variations in delays. As we will discuss later, this scheme has intriguing characteristics which complement the SIC logic. Therefore the study includes DS along with the main theme of the work, SIC. We will return to DS further in the experimental validation section.

It is important to note that both methods (SIC and DS) require a precise knowledge of the stable operating regions in the delay space, i.e., the *stability maps*. These regions (also known as 'stability pockets'), can be exhaustively obtained using the CTCR paradigm (see Appendix A).

3.2 Sign Inverting Control for Single-delay Systems

To illustrate the concept of the paradoxical control concept, Sign Inverting Control (SIC), we first study the time-delay system with only one delay. For this, a MATLAB code is developed to reveal the stability feature of the single-delay systems with arbitrary degree of order (see Appendix B). The code can be easily modified to check the effect of Sign Inverting Control for linear time invariant single-delay systems. We take one example as

$$\mathbf{A}=\begin{bmatrix} 0 & 1 & 0 & 0 \\ -40 & -2 & 20 & 0 \\ 0 & 0 & 0 & 1 \\ 3 & 0 & -30 & -1 \end{bmatrix}, \quad \mathbf{B}=\begin{bmatrix} 0 & 0 & 0 & 0 \\ 14 & 0 & 1.4 & 0 \\ 0 & 0 & 0 & 0 \\ 0.2 & 0 & 6 & 0 \end{bmatrix} \tag{3.3}$$

The characteristic equations for $\mathbf{B}$ and $-\mathbf{B}$ (SIC) are given respectively as:

$$CE(s,\boldsymbol{\tau}) = s^4 + 3s^3 + 72s^2 + 100s + 1140 + (20s^2 + 26s + 668.2)e^{-\tau s} + 83.72e^{-2\tau s} = 0 \tag{3.4}$$

$$\overline{CE}(s,\boldsymbol{\tau}) = s^4 + 3s^3 + 72s^2 + 100s + 1140 - (20s^2 + 26s + 668.2)e^{-\tau s} + 83.72e^{-2\tau s} = 0 \tag{3.5}$$

The developed MATLAB code based on the CTCR paradigm efficiently determines the stability outlook of the systems (3.4) and (3.5) as in Table 3. Note that SIC scheme brings in extra stable operating regions to the dynamics. Thus, the objective of increasing the delay robustness of the system by using SIC is fulfilled.

Table 3. Stability charts for system (3.3)

Stability pockets	τ range ($\mathbf{B}$)	τ range ($-\mathbf{B}$): SIC
1	[0, 0.18]	[0, 0.72]
2	[0.57, 1.20]	[0.74, 0.75]
3	[1.23, 1.32]	[1.29, 1.67]
4	[2.02, 2.15]	[1.71, 1.89]
5	[2.19, 2.47]	[2.74, 3.04]
6	[3.46, 3.61]	–

3.3 Necessary and Sufficient Conditions

As mentioned above, one can deploy the CTCR paradigm for both systems to create the respective stability maps exhaustively and non-conservatively in the delay space, $\boldsymbol{\tau} \in \Re^{l+}$. The interconnection between the two stability maps brings us to this study. Furthermore, one wonders if it is possible that this seemingly simple sign inversion yields *alternative* stable regions in the delay space. In what follows we present a series of theorems and remarks treating these questions.

Theorem 4: Let the sets of delay compositions, $\boldsymbol{\tau}$, for which the LTI-MTDS in (1.2) and (1.5) are asymptotically stable, be denoted by $\mathcal{N}$ and S, respectively. In order for polarity reversal to produce alternate stable zones, the following four conditions are necessary and sufficient.

(i) $\mathcal{N} \neq \emptyset$;

(ii) $S \neq \emptyset$;

(iii) $S \not\subset \mathcal{N}$;

(iv) $(\mathcal{N} \cup S) \setminus (\mathcal{N} \cap S) \neq \emptyset$ (i.e. the symmetric difference of $\mathcal{N}$ and S are nonempty).

Proof. The proof of this theorem is by contradiction. If either (i) or (ii) is false the corresponding regime would have no delay tolerance to start with.

If (iii) is false, no additional delay robustness is introduced by the proposed polarity reversal. If (iv) is false, it means that $S \equiv \mathcal{N}$, as a degenerate case. That means the stable operating delay set remains invariant from the original system (1.2) to its inverted companion (1.5). Therefore sign inversion does not offer any additional alternate stable operating regions.

This proves the necessary condition. Sufficiency clause is self-evident. If the four conditions are satisfied, it is sufficient to declare that alternative stable regions could be achieved by inverting the polarity of the delayed states. ♦

Theorem 4 reveals the necessary and sufficient condition for SIC to be feasible, i.e., the original system (1.2) and the inverted one (1.4) have complementary stability maps in the delay domain.

3.4 Main Results: Effects of Polarity Reversal on Delay-Dependent Stability Characteristics

We start by defining a similar frequency set as in (1.5) but this time for the system with reversed polarity

$$\overline{\mathbf{\Omega}} = \{\omega_c \mid \overline{CE}(s = \omega_c i, \boldsymbol{\tau}) = 0, \ \ \boldsymbol{\tau} \in \Re^{l+}, \ \ \omega_c \in \Re^{+}\} \tag{3.1}$$

Theorem 5: *Invariance property for imaginary spectra.* Between the original and inverted systems, the imaginary spectra remain invariant. That is, $\mathbf{\Omega} \equiv \overline{\mathbf{\Omega}}$.

Proof: Assume that for a given delay set $\boldsymbol{\tau}_0 = (\tau_{10}, \tau_{20}, ..., \tau_{l0}) \in \Re^{l+}$, (1.3) has an imaginary root pair $s = \pm\omega_c i$. That is,

$$CE(\omega_c i, \boldsymbol{\tau}_0) = \det\left(\omega_c i\mathbf{I} - \mathbf{A} - \sum_{i=1}^{l} \mathbf{B}_\mathbf{i} e^{-\tau_{i0}\omega_c i} \right) = 0 \tag{3.2}$$

and therefore $\omega_c \in \mathbf{\Omega}$. The theorem claims that (1.4) possesses the same imaginary root pair with (1.2) but for a different delay set. In order to prove this, consider a shifted delay set $\boldsymbol{\tau}_0 + \mathbf{g}\pi/\omega_c$,

$\mathbf{g} = [(2g_1+1),(2g_2+1),...,(2g_l+1)]$ where $g_1, g_2, ..., g_l$ are integers. For this new delay set $\boldsymbol{\tau}_0 + \mathbf{g}\pi/\omega_c$, we test the imaginary root pair $s = \pm\omega_c i$ as a potential root

$$\overline{CE}(\omega_c i, \boldsymbol{\tau}_0 + \mathbf{g}\frac{\pi}{\omega_c}) = \det\left(\omega_c i\mathbf{I} - \mathbf{A} + \sum_{i=1}^{l}\mathbf{B_i}e^{-\tau_{i0}\omega_c i}e^{-2g_i\pi i}e^{-\pi i}\right) = 0 \tag{3.3}$$

which further reduces to

$$\overline{CE}(\omega_c i, \boldsymbol{\tau}_0 + \mathbf{g}\frac{\pi}{\omega_c}) = \det(\omega_c i\mathbf{I} - \mathbf{A} - \sum_{i=1}^{l}\mathbf{B_i}e^{-\tau_{i0}\omega_c i}) \tag{3.4}$$

Comparing (3.4) and (3.2), one arrives at

$$\overline{CE}(\omega_c i, \boldsymbol{\tau}_0 + \mathbf{g}\frac{\pi}{\omega_c}) = CE(\omega_c i, \boldsymbol{\tau}_0) = 0 \tag{3.5}$$

We conclude for the two systems (1.2) and (1.4), $\boldsymbol{\Omega} \equiv \overline{\boldsymbol{\Omega}}$ with a nuance that the corresponding delays have odd multiples of π/ω_c shift from one to the other. ♦

Theorem 6: ***Root tendency invariance with respect to the polarity of the delayed state.*** If for a given delay set $\boldsymbol{\tau}_0 = (\tau_{10}, \tau_{20}, ..., \tau_{l0}) \in \Re^{l+}$, the original system (1.2) has an imaginary root pair $s = \pm\omega_c i$ with a corresponding $RT|_{s=\omega i}^{\tau_j}$, the inverted case (1.4) will possess the same *RT* for the delay set $\boldsymbol{\tau}_0 + \overline{\boldsymbol{\pi}}/\omega_c$, $\overline{\boldsymbol{\pi}} = (\pi, \pi, \ldots, \pi) \in \Re^l$. That is,

$$RT|_{CE,\,<\boldsymbol{\tau}_0,\,\omega_c>}^{\tau_j} = RT|_{\overline{CE},\,<\boldsymbol{\tau}_0+\overline{\boldsymbol{\pi}}/\omega_c,\,\omega_c>}^{\tau_j},\ j = 1,2,...,l \tag{3.6}$$

where $RT|_{CE,<\boldsymbol{\tau}_0,\omega_c>}^{\tau_j}$ is the *RT* of $CE(s,\boldsymbol{\tau})$ analyzed for delays $\boldsymbol{\tau}_0$ and $RT|_{\overline{CE},<\boldsymbol{\tau}_0+\overline{\boldsymbol{\pi}}/\omega_c,\omega_c>}^{\tau_j}$ is the *RT* of $\overline{CE}(s,\boldsymbol{\tau})$ for delays $\boldsymbol{\tau}_0 + \overline{\boldsymbol{\pi}}/\omega_c$.

Proof: The characteristic equation in (1.2) can be expanded in the following form:

$$CE(s,\boldsymbol{\tau}) = \sum_{i=0}^{r} P_i(s)e^{-s\sum_{k=1}^{l} n_{ik}\tau_k} \tag{3.7}$$

where $P_i(s)$ are polynomials with real coefficients and n_{ik} are non-negative integers. Without loss of generality, $P_0(s)$ is taken as the polynomial with the highest degree of *s*, since the system (1.2) is a retarded LTI-MTDS and $n_{0k} = 0$, $k = 1,2,...,l$. Similarly, (3.2) can be rewritten as

$$\overline{CE}(s,\boldsymbol{\tau}) = \sum_{i=0}^{r} (-1)^{q_i} P_i(s) e^{-s\sum_{k=1}^{l} n_{ik}\tau_k} \tag{3.8}$$

where q_i is a positive integer with the same parity as $\sum_{k=1}^{l} n_{ik}$. Without loss of generality, we prove the equivalency of the *RT* in τ_1 direction between $CE(s,\boldsymbol{\tau})$ and $\overline{CE}(s,\boldsymbol{\tau})$ first, then claim that it holds for the remaining delays as well.

We need to show that

$$RT\big|^{\tau_1}_{CE,<\boldsymbol{\tau}_0,\omega_c>} = RT\big|^{\tau_1}_{\overline{CE},<\boldsymbol{\tau}_0+\bar{\boldsymbol{\pi}}/\omega_c,\omega_c>} \tag{3.9}$$

For this we start with the following claims:

(a) $RT\big|^{\tau_1}_{CE,<\boldsymbol{\tau}_0,\omega_c>}$ is defined at point $\boldsymbol{\tau}_0$ and it remains invariant for the points $\{\tau_{10} + (2\pi/\omega_c)j, \tau_{20}, \ldots, \tau_{l0}\}$, $j = 0,1,2,\ldots$.

(b) $RT\big|^{\tau_1}_{\overline{CE},<\boldsymbol{\tau}_0+\bar{\boldsymbol{\pi}}/\omega_c,\omega_c>}$ is identical to $RT\big|^{\tau_1}_{CE,<\boldsymbol{\tau}_0,\omega_c>}$ and also remains invariant at points $\{\tau_{10} + \pi/\omega_c + (2\pi/\omega_c)j, \tau_{20} + \pi/\omega_c, \ldots, \tau_{l0} + \pi/\omega_c\}$, $j = 0,1,2,\ldots$.

The claim (a) is equivalent to Proposition 2 in the Appendix A, and thus it holds. A brief version of the proof is presented here, in preparation for claim (b). To prove (a) we keep all $l-1$ delays τ_k ($k = 2,3,...,l$) fixed and check the root sensitivity with respect to τ_1 at grid points $\{\tau_{10} + (2\pi/\omega_c)j, \tau_{20}, \ldots, \tau_{l0}\}$, $j = 0,1,2,\ldots$. It is obtained from (3.7) as

$$\left.\frac{\partial s}{\partial \tau_1}\right|_{\substack{CE \\ s=\omega_c i}} = \omega_c i \left(\frac{\sum_{i=0}^{r} P_i'(s) e^{-s\sum_{k=1}^{l} n_{ik}\tau_k} - \sum_{i=0}^{r} P_i(s) \sum_{k=2}^{l} n_{ik}\tau_k e^{-s\sum_{k=1}^{l} n_{ik}\tau_k}}{\sum_{i=0}^{r} P_i(s) n_{i1} e^{-s\sum_{k=1}^{l} n_{ik}\tau_k}} - \tau_1 \right)^{-1} \Bigg|_{s=\omega_c i} \tag{3.10}$$

where $P_i'(s) = dP_i(s)/ds$. Since exponential terms $e^{-\tau_1 s}\big|_{s=\omega_c i}$, $\tau_1 = \tau_{10} + 2\pi j/\omega_c$, $j = 0,1,2,...$ remain the same as $e^{-\tau_{10} s}$ for all the index j values, we conclude that they vary only with τ_{10} and are thus independent of j values. Since τ_{10} is constant and the remaining delays are fixed as $\tau_k = \tau_{k0}$, $(k = 2,3,..., l)$, (3.10) is reduced to

$$\left.\frac{\partial s}{\partial \tau_1}\right|_{\substack{CE \\ s=\omega_c i}} = \omega_c i \left(\frac{\sum_{i=0}^{r} P_i'(s) e^{-s\sum_{k=1}^{l} n_{ik}\tau_{k0}} - \sum_{i=0}^{r} P_i(s) \sum_{k=2}^{l} n_{ik}\tau_{k0} e^{-s\sum_{k=1}^{l} n_{ik}\tau_{k0}}}{\sum_{i=0}^{r} P_i(s) n_{i1} e^{-s\sum_{k=1}^{l} n_{ik}\tau_{k0}}} - \tau_1 \right)^{-1} \Bigg|_{s=\omega_c i}$$

$$= \omega_c i \left(H(s, \boldsymbol{\tau}_0) - \tau_1 \right)^{-1} \Big|_{s=\omega_c i} \tag{3.11}$$

where $H(s, \boldsymbol{\tau}_0)$ is apparent from (3.11) and it is invariant with respect to the values of τ_1. Taking the frequency $\omega_c > 0$ and using (3.11), we obtain

$$RT\big|_{CE, <\boldsymbol{\tau}_0, \omega_c>}^{\tau_1} = \operatorname{sgn}\left[\operatorname{Re}\left(\left.\frac{\partial s}{\partial \tau_1}\right|_{\substack{CE \\ s=\omega_c i}} \right) \right] = \operatorname{sgn}[\operatorname{Im}(H(s, \boldsymbol{\tau}_0)\big|_{s=\omega_c i})] \tag{3.12}$$

which is invariant for all $\tau_1 = \tau_{10} + 2\pi j/\omega_c$, $j = 0,1,2,....$ Thus it proves the claim (a).

Similarly, to obtain $RT\big|_{\overline{CE}, <\boldsymbol{\tau}_0 + \bar{\boldsymbol{\pi}}/\omega_c, \omega_c>}^{\tau_1}$ in claim (b), we keep $\tau_k (k = 2,3,...,L)$ fixed and check the root sensitivity with respect to τ_1. It can be obtained from (3.2) as

$$\left.\frac{\partial s}{\partial \tau_1}\right|_{\substack{\overline{CE} \\ s=\omega_c i}} = \omega_c i \left(\frac{\sum_{i=0}^{r} (-1)^{q_i} P_i'(s) e^{-s\sum_{k=1}^{l} n_{ik}\tau_k} - \sum_{i=0}^{r} (-1)^{q_i} P_i(s) \sum_{k=2}^{l} n_{ik}\tau_k e^{-s\sum_{k=1}^{l} n_{ik}\tau_k}}{\sum_{i=0}^{r} (-1)^{q_i} P_i(s) n_{i1} e^{-s\sum_{k=1}^{l} n_{ik}\tau_k}} - \tau_1 \right)^{-1} \Bigg|_{s=\omega_c i} \tag{3.13}$$

For the delay set $\boldsymbol{\tau}_0 + \bar{\boldsymbol{\pi}}/\omega_c$, we only change τ_1 to $\bar{\tau}_1 = \tau_{10} + \pi/\omega_c + (2\pi/\omega_c)j$, $j = 0,1,2,...$, while keeping the remaining $\tau_k (k = 2,3,...,l)$ fixed. Noticing that q_i and $\sum_{k=1}^{l} n_{ik}$ have the same parity, we have:

$$\begin{aligned}(-1)^{q_i} e^{-s\sum_{k=1}^{l} n_{ik}\tau_k}\Big|_{s=\omega_c i} &= (-1)^{q_i} e^{-\omega_c i\sum_{k=1}^{l} n_{ik}\tau_{k0}} e^{-\sum_{k=1}^{l} n_{ik}\pi i} \\ &= (-1)^{2q_i} e^{-\omega_c i\sum_{k=1}^{l} n_{ik}\tau_{k0}} = e^{-\omega_c i\sum_{k=1}^{l} n_{ik}\tau_{k0}}\end{aligned} \tag{3.14}$$

Thus, (3.13) reduces to:

$$\left.\frac{\partial s}{\partial \tau_1}\right|_{\substack{\overline{CE} \\ s=\omega_c i}} = \omega_c i \left(\frac{\sum_{i=0}^{r} P_i'(s) e^{-s\sum_{k=1}^{l} n_{ik}\tau_{k0}} - \sum_{i=0}^{r} P_i(s)\sum_{k=2}^{l} n_{ik}\tau_{k0} e^{-s\sum_{k=1}^{l} n_{ik}\tau_{k0}}}{\sum_{i=0}^{r} P_i(s) n_{i1} e^{-s\sum_{k=1}^{l} n_{ik}\tau_{k0}}} - \bar{\tau}_1 \right)^{-1}\Bigg|_{s=\omega_c i} \tag{3.15}$$

This expression is rewritten as

$$\left.\frac{\partial s}{\partial \tau_1}\right|_{\substack{\overline{CE} \\ s=\omega_c i}} = \omega_c i \left(H(s,\boldsymbol{\tau}_0) - \bar{\tau}_1\right)^{-1}\Big|_{s=\omega_c i} \tag{3.16}$$

which is exactly the same as (3.11) with the identical $H(s,\boldsymbol{\tau}_0)$ expression. Following statements become evident

$$\begin{aligned}RT\big|^{\tau_1}_{\overline{CE},\,<\boldsymbol{\tau}_0+\bar{\boldsymbol{\pi}}/\omega_c,\,\omega_c>} &= \operatorname{sgn}\left[\operatorname{Re}\left(\left.\frac{\partial s}{\partial \tau_1}\right|_{\substack{\overline{CE} \\ s=\omega_c i}}\right)\right] \\ &= \operatorname{sgn}[\operatorname{Im}(H(s,\boldsymbol{\tau}_0)\big|_{s=\omega_c i})] = RT\big|^{\tau_1}_{CE,\,<\boldsymbol{\tau}_0,\,\omega_c>}\end{aligned} \tag{3.17}$$

Thus, $RT\big|^{\tau_1}_{\overline{CE},<\boldsymbol{\tau}_0+\bar{\boldsymbol{\pi}}/\omega_c,\omega_c>}$ is identical to $RT\big|^{\tau_1}_{CE,<\boldsymbol{\tau}_0,\omega_c>}$. Furthermore it remains invariant with respect to the values of τ_1 where $\tau_1 = \tau_{10} + \pi/\omega_c + (2\pi/\omega_c)j$, $j = 0,1,2,...$, due to the Proposition 2 in the Appendix A. In short, before and after the sign inversion, *RT* remains invariant at the corresponding points on $\wp$. ♦

Remark 5: We wish to emphasize that the *RT* property (3.17), and its invariance proven in Theorem 6, strictly concern the *direction* of root crossings. Neither the root sensitivity $\partial s/\partial \tau_j$ nor its real part

$\mathrm{Re}\left(\partial s/\partial \tau_j\right)$ remain invariant between the original and inverted systems, but the $\mathrm{sgn}\left[\mathrm{Re}\left(\partial s/\partial \tau_j\right)\right]$ does, which is the indicator of the root transition direction.

Corollary 1: Based on Theorems 5 and 6 the following is true: In order to create $\mathcal{N}$ and S stability sets *only the kernel set of the original system and its RT's* are needed. The kernel hypersurfaces corresponding to (1.2) are finite as proven by Proposition 1 in the Appendix A. Then the kernel hypersurfaces of the system with inverted polarity (1.4) are simply obtained from the former by π/ω_c shifts along the axes of the delays while the *RT*s remain invariant.

Theorem 7: Sign inversion generates a building block shifting of $\Delta(\boldsymbol{\tau}\omega_c) = (\pi, \pi, \ldots, \pi) \in \Re^l$ in SDS.

Proof: From Theorem 5, for kernel and offspring hypersurfaces, the delayed state sign inversion creates a point-wise shift of $\boldsymbol{\tau} \to \boldsymbol{\tau} + \bar{\boldsymbol{\pi}}/\omega_c$. When these hypersurfaces are displayed on SDS, the respective shift occurs as $\boldsymbol{\tau}\omega_c \to \boldsymbol{\tau}\omega_c + \bar{\boldsymbol{\pi}}$. ♦

This feature, along with the stackability of the building block (see Section 2.2.1), brings a noticeable computational advantage in the exhaustive determination of kernel and offspring hypersurfaces.

3.5 Example Case Study

In order to demonstrate the effect of the polarity inversion on stability characteristics of the system, we take an example case as

$$\mathbf{A}=\begin{pmatrix}-5.4 & 6.3\\ -6 & 5.8\end{pmatrix},\quad \mathbf{B}_1=\begin{pmatrix}0.192 & 0\\ 0.348 & 0\end{pmatrix},\quad \mathbf{B}_2=\begin{pmatrix}0 & -0.324\\ 0 & -0.384\end{pmatrix} \tag{3.18}$$

The corresponding characteristic equation is

$$\begin{aligned}CE(s,\boldsymbol{\tau}) = {} & s^2-0.4s+6.48+(-0.192s-1.0788)e^{-\tau_1 s}\\ & +(0.384s+0.1296)e^{-\tau_2 s}+0.039024e^{-(\tau_1+\tau_2)s}\end{aligned} \tag{3.19}$$

Notice that (3.18) has some specific features: $rank(\mathbf{B}_1)=rank(\mathbf{B}_2)=1$, $rank(\mathbf{B}_1+\mathbf{B}_2)=2$. It leads to an interesting phenomenon known as the cross-talk of delays, i.e. $e^{-(\tau_1+\tau_2)s}$. Inverting the signs of $\mathbf{B}_1$ and $\mathbf{B}_2$, the resulting characteristic equation becomes

$$\begin{aligned}\overline{CE}(s,\boldsymbol{\tau}) = {} & s^2-0.4s+6.48+(0.192s+1.0788)e^{-\tau_1 s}\\ & -(0.384s+0.1296)e^{-\tau_2 s}+0.039024e^{-(\tau_1+\tau_2)s}\end{aligned} \tag{3.20}$$

For both (3.19) and (3.20), the imaginary spectra are calculated identically as $\boldsymbol{\Omega}=[2.17,\ 2.92]\,\text{rad/s}$ which is expected due to Theorem 5. Using the CTCR paradigm, the SDS representations of the kernel and offspring are shown in Fig. 4 for both polarities. It is clear that the inversion results in a shift of the building block by π in both $\tau_1\omega$ and $\tau_2\omega$ directions. The combined stability map in delay space is then obtained as shown in Fig. 5. The red curves in Fig. 5 are the kernels and the blue curves represent the offspring. Sample root tendencies are marked to display the invariance properties as discussed in Theorem 6. The stable regions contributed by the original and inverted systems are distinguished with different tones of shading.

It can be seen from Fig. 5, both systems are unstable when there is no delay. The stability for both systems is recovered, however, by simply increasing the delays to the available "stable pockets". Both systems provide some stable delay compositions satisfying conditions i and ii of Theorem 4. Furthermore $S\not\subset\mathcal{N}$ (condition iii) and the symmetric difference of S and $\mathcal{N}$ is nonempty (condition iv) are satisfied as shown in Fig. 5. All four necessary and sufficient conditions in Theorem 1 are fulfilled. Hence polarity inversion provides alternative stable regions in delay space. It is shown that reversing the polarity of the

retarded terms in the dynamics can improve robustness against delays considerably under four necessary and sufficient conditions provided by Theorem 4.

3.6 Relationship between the SIC Kernel and Original Kernel

In this subsection, we study the relationship between the Kernel Hypersurfaces (KH) of the SIC applied systems and those of the original systems.

Lemma 5: Given KH, i.e., $\wp_0$, for the original system, the KH for the SIC system are obtained as

$$\wp_0^{SIC} = \left\{ \begin{array}{r} \boldsymbol{\tau} + \frac{\pi}{\omega}[(-1)^{n_1},(-1)^{n_2},...,(-1)^{n_l}] \,|\, \boldsymbol{\tau} \in \wp_0,\ n_k = 1 \ if\ \tau_k \geq \frac{\pi}{\omega}; \\ n_k = 0 \ if\ 0 < \tau_k < \frac{\pi}{\omega}, k = 1,2,...,l \end{array} \right\} \tag{3.18}$$

Proof: According to Theorem 5 (*Invariance property for imaginary spectra*) in the subsection 3.4, $\boldsymbol{\Omega} \equiv \boldsymbol{\Omega}_{SIC}$ and the original system becomes SIC systems when all the delays are shifted by π/ω. Thus, the points on kernel and offspring hypersurfaces (KOH) of SIC applied system are obtained just by shifting those of original system by π/ω in a point-wise sense. However, the shifted points on KOH of original system must contain no negative delay components to form the points on KOH of SIC system. Thus, each delay component of the points on KOH of original system should be checked against π/ω and be modified accordingly in a point-wise sense as shown in (3.18). ♦

Theorem 8: The stability map of the SIC system can be obtained from that of the original system.

Proof: If the stability map for the original system is available, $\wp_0$ and their $RT's$ information are known. As per Lemma 5, $\wp_0^{SIC}$ can be obtained from (3.18). Furthermore, $\wp^{SIC}$ can be obtained from (2.3). Thus, the KOH for the SIC applied system are available by combining $\wp_0^{SIC}$ and $\wp^{SIC}$.

According to Theorem 5 (RT *invariance in SIC*), the RT for a point on $\wp_0^{SIC}$ is identical to that for the corresponding point on $\wp_0$. That is, the RT information for the SIC system can be extracted from that of the original system without the need for explicit calculation. With the needed knowledge of $\wp_0^{SIC}$, $\wp^{SIC}$ and the RT information for each point on $\wp_0^{SIC}$, we follow the steps below to get the stability map for the SIC system:

(1) Determine the stability feature of the non-delayed SIC system, $\boldsymbol{\tau} = \mathbf{0}$ (i.e., the origin).

(2) Traverse through various line segments that are parallel to one of the coordinates of $\boldsymbol{\tau} \in \Re^{l+}$ domain to connect the origin to any point of interest in the delay space. During this transition, we use RT invariance property (Proposition 2 in Appendix A) for the SIC system and implement the D-Subdivision method [27] to obtain the number of unstable roots (NU) for the entire $\boldsymbol{\tau} \in \Re^{l+}$ domain.

(3) Claim those regions in $\boldsymbol{\tau} \in \Re^{l+}$ domain where NU=0 as stable regions. ♦

Corollary 2: For any point $\boldsymbol{\tau} = (\tau_1, \tau_2, ..., \tau_l) \in \wp_0$ of the retarded original time delay system (1.2) and the corresponding point $\boldsymbol{\tau}' = (\tau_1', \tau_2', ..., \tau_l') \in \wp_0^{SIC}$ as per (3.18) of the SIC system, we have the inequality condition $\tau_i' \neq \tau_i$, $i = 1,2,...,l$.

Proof: For the retarded time delay system, an upper bound of the imaginary spectrum exists [48]. That is, the crossing frequency set does not contain infinity and thus the offset value π/ω in (3.18) is guaranteed to be a nonzero value. In other words, each delay component of a point on $\wp_0^{SIC}$ is shifted by a nonzero value from the corresponding point on $\wp_0$. That is, $\tau_i' = \tau_i \pm \pi/\omega, i = 1,2,...,l$ where $\pi/\omega \neq 0$. Thus, $\tau_i' \neq \tau_i, i = 1,2,...,l$. ♦

Definition 6: *Edge Point: a* point on KH, $\wp_0$, where one or more of the delays $\tau_k, k = 1,2,..l$ become zero, which create a discontinuity of $2\pi/\omega$ on the KH. ■

Definition 7: *Classification of KH* $\wp_0$: (a) $\wp_0^1$ *Class:* one closed KOH; (b) $\wp_0^2$ *Class:* one contiguous KH with edge points; (c) $\wp_0^3$ *Class:* several contiguous KH with edge points. We denote the multiple segments of $\wp_0^i$ $(i = 1,2,3)$ for (1.2) by $\wp_0^{i(j)}$ $(i = 1,2,3;\ j = 1,2,3,4...)$. The corresponding segments of KH $\wp_0^{i(j)}$ for SIC system are denoted by $\wp_0^{SIC\_i(j)}$. ■

Theorem 9: The number of the edge points of $\wp_0^{SIC\_i(j)}$ $(i = 1,2,3;\ j = 1,2,3,4...)$ is twice the number of the occurrences of $\tau_k = \pi/\omega, k = 1,2,..l$ for $\wp_0^{i(j)}$. Also, the edge points have the offset value $2\pi/\omega$ along τ_k axis.

Proof: According to (1.3), if a point, say $\boldsymbol{\tau}_A = (\tau_1, \tau_2, ..., \tau_k, ..., \tau_l)$ on $\wp_0^{i(j)}$ $(i = 1,2,3;\ j = 1,2,3,4...)$ has the delay component $\tau_k = \pi/\omega_A$, it is mapped to the corresponding point $\boldsymbol{\tau}_{B'} = (\tau_1', \tau_2', ..., 0, ..., \tau_l')$ on $\wp_0^{SIC}$. Then the point $\boldsymbol{\tau}_{B'} = (\tau_1', \tau_2', ..., 2\pi/\omega_B, ..., \tau_l') \in \wp^{SIC}$ is also on $\wp_0^{SIC}$ as per (2.2) and is adjacent to $\wp^{SIC}$. If

the point B' is not adjacent to $\wp^{SIC}$, it exhibits a discontinuity between $\wp_0^{SIC}$ and $\wp^{SIC}$ which contradicts the D-Subdivision method (or the "continuity argument") [27]. Therefore, one occurrence of $\tau_k = \pi/\omega_B,\ k = 1,2,..l$ for $\wp_0^i$ corresponds to two edge points on $\wp_0^{SIC}$ (i.e., B' and B'') and notice that the distance of B' and B'' along τ_k is $2\pi/\omega_B$. The above analysis applies to the other points on $\wp_0^{i(j)}$ as well and thus the theorem is proven. ♦

Corollary 3: If $\wp_0^{i(j)}$ $(i = 1,2,3;\ j = 1,2,3,4...)$ has no occurrence of $\tau_k = \pi/\omega,\ k = 1,2,..l$, the corresponding $\wp_0^{SIC\_i(j)}$ is closed.

Proof: From Theorem 9, if no occurrence of $\tau_k = \pi/\omega,\ k = 1,2,..l$ is observed for $\wp_0^{i(j)}$, the corresponding $\wp_0^{SIC\_i(j)}$ has no edge points and thus is closed. ♦

Corollary 4: The number of open contiguous KH of $\wp_0^{SIC}$ that corresponds to $\wp_0^{i(j)}$ $(i = 1,2,3;\ j = 1,2,3,4...)$ of the original system is equal to the number of intersection points of $\tau_k\omega - \pi, k = 1,2,...,l$ with zero when $\wp_0^{i(j)}$ is continuously swept.

Proof: The number of intersection points of $\tau_k\omega - \pi, k = 1,2,...,l$ with zero while sweeping $\wp_0^{i(j)}$ continuously is equal to the number of occurrences of $\tau_k = \pi/\omega,\ k = 1,2,..l$ for $\wp_0^{i(j)}$. From Theorem 9, this number is one half the number of the edge points of $\wp_0^{SIC\_i(j)}$. Since two edge points correspond to one contiguous KH, the number of occurrences of $\tau_k = \pi/\omega,\ k = 1,2,..l$ for $\wp_0^{i(j)}$ equals the number of contiguous KH. Therefore, the corollary is proven. ♦

The Corollary 4 actually provides a feasible way to check the number of open contiguous KH of $\wp_0^{SIC}$ that corresponds to $\wp_0^{i(j)}$.

4. Optimal Sign Inverting Control for Multiple Time-delay Systems

4.1 Introduction

Sign Inverting Control (SIC) with large delays may yield some complementary benefits to the original control logic from delay robustness perspective. The main question we address in this chapter is "How to select the original control law so that such a contribution can be (a) feasible, (b) optimal in some sense?" A structured methodology is proposed to achieve this, starting with an LQR (Linear Quadratic Regulator)-based controller. A single scaling factor on the corresponding control gains is used for 1-D optimization.

Consider the dynamics of the system with non-delayed feedback control as

$$\dot{\mathbf{x}} = \mathbf{A}\mathbf{x} - \bar{\mathbf{B}}\mathbf{K}\mathbf{x} \tag{4.1}$$

This "original control law" should be assigned such that the system has a desirable control performance (for example, disturbance rejection or tracking ability). Uncontrolled system (i.e., $\mathbf{K} = \mathbf{0}$) is therefore assumed to be asymptotically stable. When $|\mathbf{K}|$ is very small (which implies that each component is infinitesimally small), the dynamics is expected to be still asymptotically stable. Even when time delays occur in the feedback line, the dynamics with infinitesimally small feedback gains should remain "delay independent stable" [49]. A rationale for this is that the control signal is so feeble that the inherent uncontrolled dynamics dominate the close-loop response. However as $|\mathbf{K}|$ increases, the stability property becomes delay dependent which means that the system is asymptotically stable only for some delay compositions.

To design an original control law, we use the well-known LQR procedure for the non-delayed dynamics, which guarantees stability and optimality in the control performance and power usage perspective. Time

delays are then introduced into the control feedback line. Expectedly, if we take an LQR-based controller as the original control law, the corresponding SIC exhibits no (or very little) tolerance against delays. The reason for this is that the control actuation created by gain K is designed to be so strong to impose optimum tracking that the system cannot tolerate delays. To remedy this, we propose a parametric scaled-down control design methodology starting from LQR results. We show that this methodology can create desirable delay robustness.

In short, the controller design is performed through the following steps:

(a) First, a full-state feedback control law $(\mathbf{K})$ is selected based on LQR conventions for the non-delayed case. It achieves high level tracking ability using minimal control effort. But the LQR controller is expectedly very poor when it comes to delay robustness.

(b) We then consider delays in the control structure. For this system, CTCR paradigm creates an exclusive stability map in the space of the delays.

(c) For the SIC applied system, we obtain a new stability map, again using CTCR, for SIC, and compare it with the one obtained for the original control logic in (b).

(d) If the stability maps obtained in (b) and (c) fail to satisfy the necessary and sufficeint conditions stated in Theorem 4, we scale down the control gain $(\mathbf{K})$. Instead of changing all the entries of $\mathbf{K}$ randomly, we introduce a control gain scaling parameter $\alpha \in [0,1]$ such that the new control gain becomes

$$\mathbf{K}' = \alpha \mathbf{K}$$

With this new gain we repeat the procedures (b) and (c). It is intuitively obvious that the smaller this scaling parameter α, the larger the delay robustness. For $\alpha \approx 0$, the stability becomes delay independent (as the feedback control which carries the delays vanishes). As such, the system presents infinite delay robustness. But then the controller is effectively inexistent, and the tracking ability disappears.

(e) This iterative process is ceased when the stable regions of (b) and (c) satisfy the necessary and sufficient conditions in Theorem 4.

4.2 Optimality of SIC Scheme

It is clear that $\alpha = 1$ is optimum in LQR sense for tracking ability, and $\alpha = 0$ offers delay independent stability. In order to bring a compromising trade-off scenario, $\alpha \in [0,1]$ is selected large enough such that a balance is established between the delay robustness and the tracking ability. To achieve this, we formulate an objective function to be minimized which is composed of two parts:

(i) First component, y_1, is the reciprocal of the area of the stable operating zones in the delay space (i.e., $(Area_{stable})^{-1}$). The larger the stable area in delay space (i.e., the smaller the reciprocal) the more preferred the selection becomes from the delay robustness perspective. Clearly y_1 is a function of α.

(ii) Second component, y_2, has to do with the dominant settling time for the *non-delayed* dynamics of (4.1) which is a measure of tracking ability. This dominant settling time (or the corresponding time constant) is again a function of α.

(iii) A combined objective function to be minimized is defined as $y = \beta y_1 + y_2$, where β is a positive, user-selected weighting factor in order to bring the desired balance between the two competing objectives. This objective function is numerically well-defined as a function of α, i.e., $y = y(\alpha)$. The goal for optimization here is to select the control gain scaling parameter α^*, $\alpha^* \in [0,1]$ such that $y(\alpha^*)$ exhibits a minimum.

This parametric selection scheme for the optimal control is numerically well defined. The only critical element is to determine $Area_{stable}$ as the parameter $\alpha \in [0,1]$ is numerically varied. This task is handled very efficiently using the CTCR paradigm as described in the Appendix A.

5. An Experimental Case Study for Optimized SIC

To validate the described optimal SIC concept in the previous chapter, tests are conducted on a single-axis manipulator setup (an actuated pendulum) as shown in Fig. 6. The trajectory tracking performance of the pendulum with/without delays is investigated. A desired trajectory is selected arbitrarily without violating the torque and bandwidth limitations of the actuator. The actuator we used is a DC servo-motor (Minertia Motor, FB5L20E) equipped with an optical encoder (with 4000 pulses per revolution) which measures the pendulum angle, θ, from its equilibrium position. The control sampling speed used in the experiments is 1000 Hz. The linearized state space representation of this dynamics is taken from [50]

$$\dot{\mathbf{x}} = \mathbf{A}\mathbf{x} + \overline{\mathbf{B}} V_a \tag{5.1}$$

$$\mathbf{x} = \begin{bmatrix} \theta \\ \dot{\theta} \end{bmatrix}, \quad \mathbf{A} = \begin{bmatrix} 0 & 1 \\ -\dfrac{mgl}{2J} & -\dfrac{b + \dfrac{K_b K_i}{R_a}}{J} \end{bmatrix}, \quad \overline{\mathbf{B}} = \begin{bmatrix} 0 \\ \dfrac{K_i}{R_a J} \end{bmatrix}$$

where V_a is the control voltage (motor armature voltage) and the other electro-mechanical properties of the motor-pendulum setup are listed in Table 4.

Table 4. Parameters of the experimental setup

Parameter	**Value**	**Unit**
m (pendulum mass)	0.125	kg
l (pendulum length)	0.33	m
g (gravitational constant)	9.807	m/s^2
J (rotational inertia)	0.0042	kgm^2
R_a (armature resistance)	3.4	Ω
K_b (back-emf constant)	0.0592	Vs/rad
K_i (torque constant)	0.0592	Nm/A
b (torsional damping coefficient)	0.0045	Nms/rad

The control structure shown in Fig. 7 is implemented for trajectory tracking. A combination of feed-forward and feedback control is used. The feed-forward logic is obtained as follows:

$$\dot{\mathbf{x}}_d = \mathbf{A}\mathbf{x}_d + \overline{\mathbf{B}} V_d \tag{5.2}$$

$$V_d = \frac{R_a J}{K_i}\left(\ddot{\theta}_d + \frac{b + \frac{K_b K_i}{R_a}}{J}\dot{\theta}_d + \frac{mgl}{2J}\theta_d \right)$$

where $\mathbf{x}_d = [\theta_d, \dot{\theta}_d]'$ is the desired trajectory and V_d is the feed-forward control voltage. One should pay attention that the amplitude of θ_d remains within the linearity bounds of (5.1). Subtracting (5.1) from (5.2) yields the error dynamics as

$$\dot{\mathbf{e}} = \mathbf{A}\mathbf{e} + \overline{\mathbf{B}}(V_d - V_a) = \mathbf{A}\mathbf{e} + \overline{\mathbf{B}}u \tag{5.3}$$

where $\mathbf{e} = [\theta_d - \theta, \dot{\theta}_d - \dot{\theta}]'$ is the state vector describing the errors, and the full state feedback control law is selected as $u = V_d - V_a = -\mathbf{K}'\mathbf{e}$ with $\mathbf{K}' = \alpha\mathbf{K}$ and the control gain scaling parameter α. Here $\mathbf{K}$ is determined using the conventional LQR optimizer. Typically such a feedback control law does not provide meaningful delay robustness, as discussed earlier. Naturally, the SIC which corresponds to $\alpha = 1$ (unscaled but sign inverted LQR controller) is expected to be even worse. It may not manifest any delay tolerance at all (including small delays). This expectation arises from the fact that the LQR controller is optimized for tracking ability and therefore it is too strong to allow sign inversion without introducing instability. We therefore pursue a compromising parametric controller design with less aggressive gain structure $\alpha \in [0,1]$ as described in the previous chapter.

In order to test the stability robustness on the experimental setup against fixed delays, we consider a two-delay combination: τ_1, in the feedback line of angular position, θ, and τ_2, in the line of angular velocity, $\dot{\theta}$. Then, the control logic u becomes

$$u = -\mathbf{K}_1\mathbf{e}(t-\tau_1) - \mathbf{K}_2\mathbf{e}(t-\tau_2) \tag{5.4}$$

where the feedback control law $\mathbf{K}$ is conveniently separated into two segments,

$$\mathbf{K} = [k_1, k_2] \ , \ \mathbf{K}_1 = [k_1, 0] \ , \ \mathbf{K}_2 = [0, k_2] \tag{5.5}$$

The corresponding error dynamics for the delayed control system becomes

$$\dot{\mathbf{e}} = \mathbf{A}\mathbf{e} + \mathbf{B}_1\mathbf{e}(t-\tau_1) + \mathbf{B}_2\mathbf{e}(t-\tau_2) \tag{5.6}$$

where $\mathbf{B}_1 = -\overline{\mathbf{B}}\mathbf{K}_1$ and $\mathbf{B}_2 = -\overline{\mathbf{B}}\mathbf{K}_2$. Equation (5.6) represents a general class of LTI-TDS with two rationally independent delays.

The objective in our experiments is to follow a desired trajectory which is selected as a dual harmonic function with two arbitrarily selected (and even irrational) frequencies:

$$\theta_d = 0.04\sin(3\pi t) + 0.06\sin(3\sqrt{3}\pi t) \ rad \tag{5.7}$$

The described pendulum has a natural frequency of $1.1\,Hz$. Utilizing the parameters of Table 4 in (5.1), the governing dynamics is obtained with the system and control matrices as

$$\mathbf{A} = \begin{bmatrix} 0 & 1 \\ -47.6100 & -2.5493 \end{bmatrix}, \qquad \overline{\mathbf{B}} = \begin{bmatrix} 0 \\ 4.0984 \end{bmatrix} \tag{5.8}$$

As the *original* control logic to start with, we use an LQR-optimized controller. This control logic should reject the disturbances effectively. The LQR algorithm determines the feedback control gain $\mathbf{K}$ to minimize a linear quadratic cost function J

$$J = \int_0^\infty (\mathbf{e}^{\mathbf{T}}\mathbf{Q}\mathbf{e} + Ru^2)dt \tag{5.9}$$

where $\mathbf{Q}$ is a positive definite matrix and $R \in \Re^+$ is the cost factor for the control effort. In this study, they are selected as follows:

$$\mathbf{Q} = \begin{bmatrix} 300 & 0 \\ 0 & 20 \end{bmatrix}, \qquad R = 1 \tag{5.10}$$

The resulting LQR optimum feedback control law is determined (using standard MATLAB routines) as:

$$u = -\mathbf{Ke}, \quad \text{where} \quad \mathbf{K} = [9.2733 \quad 4.6434] \tag{5.11}$$

The corresponding $\mathbf{B}_1$ and $\mathbf{B}_2$ become

$$\mathbf{B}_1 = \begin{bmatrix} 0 & 0 \\ -37.8634 & 0 \end{bmatrix}, \qquad \mathbf{B}_2 = \begin{bmatrix} 0 & 0 \\ 0 & -19.0293 \end{bmatrix} \tag{5.12}$$

and the ensuing characteristic equation for the dynamics in (5.6) becomes

$$CE(s, \tau_1, \tau_2) = s^2 + 1.3018s + 47.61 + 37.8634e^{-\tau_1 s} + 19.0293s\, e^{-\tau_2 s} \tag{5.13}$$

When SIC logic is performed, the signs of $\mathbf{B}_1$ and $\mathbf{B}_2$ matrices are inverted and the characteristic equation appears as

$$\overline{CE}(s, \tau_1, \tau_2) = s^2 + 1.3018s + 47.61 - 37.8634e^{-\tau_1 s} - 19.0293se^{-\tau_2 s} \tag{5.14}$$

The superposed stability map of (5.13) and (5.14) in the delay space for the original control is obtained using the CTCR paradigm as shown in Fig. 8, where the red/green curves are the kernel, and blue/black curves are the offspring corresponding to original and SIC control logics, respectively. Take note that one of the key contributions of this study is the "large" delays. To elucidate this point further, we take two frequency components in the desired trajectory as $1.5\,Hz$ and $2.6\,Hz$ which correspond to periods of 0.66s and 0.38s, respectively. The delay ranges considered are $0 < \tau_1 < 1s$, $0 < \tau_2 < 0.5s$ which are apparently "large" compared with the frequency contents of the controlled task. The resulting control logic yields an optimized trajectory tracking performance but very limited delay robustness. As expected, the corresponding SIC controller with $\alpha = 1$ generates a characteristic equation $\overline{CE}(s, \tau_1, \tau_2)$ which is unstable for all delay compositions. This violates the second condition of Theorem 4, eliminating the possibility of expanding the use of SIC strategy for $\alpha = 1$. In order to overcome this limitation, the proposed parametric controller design method is utilized. It adjusts the control gain *scaling parameter* α in order to invite some additional delay robustness capability for the corresponding SIC. The superposed stability map for $\alpha = 0.35$ is shown in Fig. 9. Comparing the Figures 8 and 9 it is clear that the delay robustness of SIC for $\alpha = 0.35$ is much larger than that for $\alpha = 1$, and inexistent stable delay regions for

SIC case of Fig. 8 now appears with a large area in Fig. 9 in return for a reduced scaling factor ($\alpha = 0.35$). Furthermore the stability regions in Fig. 9 are complementary which satisfies the third and fourth conditions of Theorem 4.

Repeating the same exercise for varying α values, we now seek an optimum selection. For this we evaluate the reciprocal of the stable area (representing the delay robustness) as a function of α as shown in Fig. 10. Apparently, the smaller this reciprocal, the better the delay robustness is.

Then the disturbance rejection capability, which is evaluated as the dominant settling time for non-delayed dynamics (5.3) as a function of α, is generated as shown in Fig. 11. And the settling time is approximated as four times the dominant time constant.

Following step (iii) in Section 4.2, the objective function is defined as $y = \beta y_1 + y_2$ where β is a positive weighting factor as described earlier. For the compatibility of the two terms in y we select $\beta = 0.046$ here and continue with the tests.

The complete objective function variation is shown in the Fig. 12. It is visible that it favours larger α scaling factors, although the variations beyond 0.65 do not bring a noticeable advantage. In order to compare the performance of the control and the delay robustness capability for the optimum $\alpha^* = 0.65$ and suboptimal $\alpha's$ (here we take $\alpha = 0.35$ and $\alpha = 0.95$), the stability maps and the corresponding experimental results are displayed in Fig. 13 through Fig. 17.

Apparent from Figures 9, 13 and 14, as α increases, the area of the stable region and thus the delay robustness reduces. On these three stability maps, a common delay composition A ($\tau_1 = 0.3, \tau_2 = 0.06$) is arbitrarily chosen, for which all the *original* control laws remain stable.

As an important companion feature to stability, which is not the main concern in this section, is the tracking ability. It is also tested experimentally for a better understanding of the concepts introduced in this section. We conducted the tests using the optimum α^* and two suboptimum $\alpha's$. The results are shown in Figures 15 to 17 which display the closed-loop peak-to-peak tracking errors at the steady state. They are summarized in Table 5 which shows the ratio of the peak-to-peak tracking error vs peak-to-peak swings of the desired trajectory, We observe that, for a non-delayed control, larger α is preferred due to the fact that this selection brings the system closer to the optimized LQR process from tracking perspective. But this strategy provides a very small stability pocket for non-zero delays in the feedback. For such cases, $\alpha^* = 0.65$ is to yield an optimum operation for the objective function defined in Section 4.2. The operating point (A) visibly moves farther away from the nearest stability boundary when we compare Fig. 17 for $\alpha = 0.95$vs Fig. 16 for $\alpha = 0.65$. Although it is not the objective of the novelties introduced here, for the selected trajectory and the delay composition $\tau = (0.3,0.06)$ the tracking errors happens to be also in favour of the optimum scale factor $\alpha = 0.65$(as per Table 5).

Table 5. Closed-loop peak-to-peak tracking error

	$\alpha = 0.35$	$\alpha^* = 0.65$	$\alpha = 0.95$
$\tau = (0,0)$	12.3%	7.6%	7.0%
$\tau = (0.3,0.06)$	17.6%	13.4%	19.0%

The time-delayed feedback control exercises in the literature generally struggle with *small delays* which are in the order of the sampling periods (e.g., [51]) or a potential enlargement of maximum tolerable delay for stability [52]. In this thesis, however, we are proposing a completely different and paradoxical approach which considers all the stable delay pockets (thanks to CTCR procedure) and substantially enlarges them. From this angle the current work does not really have peer strategies to compare.

6. Conclusion and Future Work

6.1 Conclusions

The research in this dissertation focuses on the study of the effect of time delays in the stability of linear time delayed systems and their control strategies. The main contribution is the proposal of a novel combination of two controversial control concepts, Sign Inverting Control (SIC) and Delay Scheduling Control (DSC), for linear time invariant multiple time delayed systems (LTI-MTDS) with independent and large delays. Such multi-faceted paradoxical combinations provide previously-unexplored tools to control designers.

The contributions are validated both analytically and experimentally:

a) An important counter-intuitive finding is that controllers with large delays may yield stable operations.

b) The paradoxical SIC control concept may expand the stability region in the delay space considerably. To perform the proposed controller there are four necessary and sufficient conditions to be satisfied, and all of them can be efficiently verified using the CTCR procedure.

c) SIC may not be feasible for any arbitrary selection of the original control law. A parametric controller design methodology is developed to create a viable controller. It starts with a conventional LQR controller and scales it down to improve the delay robustness.

d) An objective function is defined to yield the optimum control with a gain scaling parameter, so that an optimum balance is achieved between the delay robustness and the tracking performance.

All of these features and properties are verified over a single-axis manipulator experimental setup in Section 5.

Specifically, Chapter 2 presents two fundamental ways to determine exhaustively the marginal stability operating points. For this, the Spectral Delay Space (SDS) and Building Block (BB) concept are introduced first. As a by-product, the Directional Root Tendency invariance property is proven within the Delay Space and the Spectral Delay Space. Another way to determine the marginal stability operating points is frequency sweeping method. The preliminary step for this technique is the exact determination of the imaginary spectral bounds, which is presented in detail.

The main contribution of this thesis, the combination of two controversial control concepts, Sign Inverting Control (SIC) and Delay Scheduling Control (DSC) is proposed in Chapter 3. In this chapter, a MATLAB code is developed to reveal the stability property of linear time-invariant single-delay systems. With this code, the performance of the SIC applied system with single delay can be examined very easily. Four necessary and sufficient conditions are outlined for SIC to be feasible. Then, several important properties of SIC scheme is presented with detailed proof. Finally, the relationship of the Kernel Hypersurfaces for the original systems and the inverted systems is studied to provide further insight of the proposed control scheme.

Chapter 4 presents one way to optimize the proposed SIC strategy with respect to the delay robustness and the control performance. An experimental case study is presented in Chapter 5 to verify the proposed control logic.

This work fills a current gap in the controller design for linear time invariant multiple time-delay systems (LTI-MTDS). The results have been shared with the scientific community in several conferences [53-56], and journal publications [33, 57, 58].

6.2 Future Work

After the completion of this dissertation there are plenty of questions that remain to be answered and that require more research to be pursued. The most evident is the necessity of a valid procedure for the controller design of the original systems so that SIC is feasible. The current work only studies delayed systems with predetermined controllers.

In addition, for the exhaustive determination of the marginal stability operating points, the proposed frequency sweeping method encountered difficulty when the number of delays or the order of systems increases. This bottleneck is due to the limited capacity of the symbolic calculations of the computer. To overcome this, more efficient algorithms are needed to reduce the need for too complicated symbolic calculations.

Finally, the topic that has not been addressed with satisfactory results is the case of switching control. When the control polarity changes in time, the resulted control performance is not only determined by the stability property of each control scheme, but also by the mechanism of switching. The interplay between the switching and the stability map needs to be explored further to have a better understanding of the role of switching control on SIC.

7. Appendix

7.1 Appendix A

Review of CTCR (Cluster Treatment of Characteristic Roots) Paradigm [29]

Consider a general class of linear time invariant, multiple time delayed systems LTI-MTDS:

$$\dot{\mathbf{x}}(t) = \mathbf{A}\mathbf{x}(t) + \sum_{j=1}^{p} \mathbf{B}_j \mathbf{x}(t - \tau_j) \tag{A.1}$$

where $\mathbf{x} \in \Re^n$, $\mathbf{A}$, $\mathbf{B}_j$ are all constant matrices in $\Re^{n\times n}$ and the all the elements of the vector of time delays $\boldsymbol{\tau} = [\tau_1, \tau_2, \cdots, \tau_p] \in \Re^{p+}$ are independent. The characteristic equation of this kind of systems is given by:

$$CE(s, \tau_1, \tau_2, \ldots, \tau_p) = \det\left(s\mathbf{I} - \mathbf{A} - \sum_{j=1}^{p} \mathbf{B}_j e^{-\tau_j s} \right) = 0 \tag{A.2}$$

The delay terms in (A.1) introduce the transcendental exponential terms in the characteristic equation (A.2), which result in infinitely many characteristic roots, i.e., the system (A.1) has infinite dimensionality. The stability analysis of the general class of multiple time delayed systems represented by (A.2) is quite intriguing, and the topic has attracted substantial attention in the control community lately. The traditional analysis tools, based on Lyapunov-Krasowskii function or the Razumikhin theorem, could only find approximate bounds for the maximum tolerable delay and the results highly depend on the selection of the function and the solution of the Linear Matrix Inequalities (LMIs).

The Cluster Treatment of Characteristic Roots, or CTCR, paradigm, collects the infinitely many characteristic roots of (A.1) into a small number of clusters, which exhibit common "clustering features". The paradigm further proves that these clusters are finite in number and furthermore they are indeed in small numbers. Appropriately processing these clusters the CTCR uniquely declares the stability maps in

the parametric domains (such as the delays). The stability switching (i.e., from stable to unstable or vice versa) occurs only at delay settings which create imaginary characteristic roots [59]. It is well known that such delays appear on infinitely many (but not dense) loci in the (τ_1, τ_2) space. The "clustering" of this insurmountable quantity of curves is achieved by the CTCR paradigm. The two crucial definitions are introduced as Definition 1-3 (i.e., Kernel Hypercurves, Offspring Hypercurves, and Root Tendency) in Chapter 2. Based on these definitions, we present two overarching propositions of the CTCR paradigm.

Definition A1. Kernel hypersurfaces $\wp_0$: The hypersurfaces in the $\Re^{p+}$ domain that exhaustively consist of all the points $\boldsymbol{\tau} \in \Re^{p+}$ which cause an imaginary root of (A.2) to have an imaginary root s=±ωi and satisfy the constraint $0<\tau_k\omega<2\pi$ are called the kernel hypersurfaces. The points on these hypersurfaces contain the smallest possible delay values that create the given pair of imaginary roots at the frequency ω.

■

Definition A2. Offspring hypersurfaces $\wp$: The hypersurfaces obtained from the kernel by the following pointwise nonlinear transformation:

$$\left\langle \tau_1 + \frac{2\pi}{\omega} j_1, \tau_2 + \frac{2\pi}{\omega} j_2 +, \cdots, \tau_p + \frac{2\pi}{\omega} j_p \right\rangle, \quad j_k = 1, 2, \ldots \tag{A.3}$$

are called the offspring hypercurves. They are created by the periodicity of the imaginary roots with respect to the time delay. ■

Definition A3. Root Tendency, RT: At any point $\boldsymbol{\tau} \in \wp_0 \cup \wp$ an infinitesimal increase in any of the individual delays, τ_j, creates a transition of the root. Such transition can be to the right or to the left half of the complex plane. The Root Tendency, RT, indicates the direction of this transition as only one of the delays, τ_j, increases by ε, $0< \varepsilon <<1$, while all the others remain constant:

$$RT\big|_{s=\omega i}^{\tau_j} = \operatorname{sgn}\left[\operatorname{Re}\left(\frac{\partial s}{\partial \tau_j} \right)\Big|_{s=\omega i} \right] \tag{A.4}$$

The following are the two overarching propositions of CTCR. They are stated without proof here, for the sake of space consideration. ■

Proposition A1: There can only be a small number of Kernel Hypersurfaces $\wp_0$. This number is upper-bounded by n^2 for a LTI-MTDS of state dimension n [21]. This is a very important feature which facilitates the creation of hypersurfaces for all possible $<\boldsymbol{\tau}, \omega_c>$ occurrences. The set $\boldsymbol{\Omega}$ is complete over this bounded number of kernel hypersurfaces.

The proof is left to [21]. We can further state that this upper bound (n^2) is very conservative and the true number of kernels would be considerably smaller.

Proposition A2: Invariant Root Tendency Property: Take an imaginary characteristic root, $\omega_c i$, paired with a delay composition $\boldsymbol{\tau}$, which really means that $<\boldsymbol{\tau}, \omega_c>$ holds. The *RT*'s of these imaginary roots remain invariant from one branch of $\wp$ to another when only one of the delays is varied. That is, *RT* with respect to the variations of a particular delay $\tau_k (k = 1,2,...,l)$ is invariant from $\wp_0$ to the corresponding offspring $\wp$ defined in (2.3) when all other delays $\tau_j (j \neq k)$ are fixed [28].

The deployment of CTCR methodology consists of two fundamental steps. The first step is to perform an exhaustive determination of the kernel set, i.e., the crossing hypersurfaces with the smallest delay values corresponding to the imaginary roots, and the corresponding root tendencies of these crossings. For this step, different methods can be used, as described in Section 2. The second step is the generation of the offspring, using the periodicity property of the crossings stated in Proposition 2, and the construction of

the stability tableau for the system. These procedures are easy and efficient to implement in a single program, allowing the generation of an exact and exhaustive stability map of the system for any arbitrarily large time delays.

7.2 Appendix B

MATLAB Code for the Stability Analysis of the Linear Time Invariant Single-delay Systems

```
% Stability analysis of x_dot=A*x+B*x(t-tau)
% This code is valid for generalized n-dimensional single delay dynamics
%% get the T values that corresponds to imaginary roots
clear all;clc;
tau_lim=35; % max limit of tau value set by user
A=[-1 13.5 -1;-3 -1 -2;-2 -1 -4];
B=[-5.9 7.1 -70.3;2 -1 5;2 0 6];
size_A=size(A,1); % size of the matrix A
syms T s e tau;
si=s*eye(size_A);
CE=det(si-A-B*e); % characteristic equation in e which is exp(-tau*s)
e=1; % let tau=0
roots_tau_zero=eval(solve(eval(CE))) % characteristic roots of the dynamics at tau=0
roots_tau_zero_r=real(roots_tau_zero); % real part
NU_tau_zero=numel(find(roots_tau_zero_r>0));
clear e; syms e; % make e symbol again
```

```
CET=subs(CE,e,(1-T*s)/(1+T*s)); % characteristic equation with Rekasiu substitution
[detn,detd]=numden(CET); % get the numerator of characteristic equation
C=sym2polys(detn,s); % get the coefficients
R=rouths(C); % Routh array of the system
rowR=size(R,1);
R1=simplify(R(rowR-1,1)); % get R1 of Routh array
[R1n,R1d]=numden(R1);
CR1n=sym2polys(R1n,T);
T=roots(double(CR1n)); % solve R1=0
T=real(T(abs(imag(T))<1e-10))
%% Solve for omega from R1=0 & R21*R22>0
[R21n,R21d]=numden(R(rowR-2,1));
[R22n,R22d]=numden(R(rowR-2,2));
sgn=sign(eval(R21n*R21d*R22n*R22d));
T=T(sgn>0); % check if R21*R22>0
R21=eval(R21n/R21d);
R22=eval(R(rowR-2,2));
omega=sqrt(R22./R21) % omega values
TAU=2./omega.*(atan(omega.*T)+pi); % corresponding tau values
for ii=1:length(TAU)
   while TAU(ii)>0
      TAU(ii)=TAU(ii)-2*pi./abs(omega(ii));
   end
   while TAU(ii)<0
      TAU(ii)=TAU(ii)+2*pi./abs(omega(ii));
   end
```

```
end % The kernel values of tau values
%% RT calculation
CEtau=subs(CE,e,exp(-tau*s)); % CE in tau
dCEdtau=diff(CEtau,tau); % partial derivative of CE wrt tau
dCEds=diff(CEtau,s); % partial derivative of CE wrt s
dsdtau=-dCEdtau/dCEds; % derivative of s wrt tau
tau=TAU;
s=omega*1i;
RT=sign(real(eval(dsdtau)))
clear tau; syms tau; % make tau symbol again
%% Obtain stability map and NU distributions
buff=0; %  for each crossing, store number of tau values within tau_lim
omega_len=length(omega);
tau_limit=zeros(omega_len,1);
maxi=0; % max number of time delays for a certain crossing to be stored for the selected max tau limit
dSdTAU=sym(zeros(omega_len,1));
for ind_lim=1:omega_len
   OMEGA=omega(ind_lim);
   tau_limit(ind_lim)=floor((tau_lim-TAU(ind_lim))/(2*pi/OMEGA))+1;
   s=1i*OMEGA;
   dSdTAU(ind_lim)=eval(dsdtau);
   if tau_limit(ind_lim)>buff
      maxi=tau_limit(ind_lim);
   else
      maxi=buff;
   end
```

```
   buff=maxi;
end
Tau=inf*ones(maxi,omega_len,3); % the 2D matrix Tau(:,:,1) is tau values; 2D matrix Tau(:,:,2) is the corresponding RT values; 2D matrix Tau(:,:,3) is the corresponding indices for omega/T values
for k=1:omega_len
   OMEGA=omega(k);
   for kk=1:1:tau_limit(k)
      Tau(kk,k,1)=TAU(k)+2*pi/OMEGA*(kk-1);
      tau=Tau(kk,k,1);
      Tau(kk,k,2)=sign(real(eval(dSdTAU(k))));
      Tau(kk,k,3)=k;
   end
end

% Puts all the time delays in an ascending order, while keeping the
% corresponding RT value for each delay
Tau1=reshape(Tau(:,:,1),maxi*length(omega),1);
Tau2=reshape(Tau(:,:,2),maxi*length(omega),1);
Tau3=reshape(Tau(:,:,3),maxi*length(omega),1);
[Tau1_sort,ind_sort]=sort(Tau1);
Tau2_sort=Tau2(ind_sort);
Tau3_sort=Tau3(ind_sort);
NUM_tau=sum(tau_limit); % number of tau values (kernel and offspring) within the tau limit
Tau1_SORT=Tau1_sort(1:NUM_tau); % truncate the sorted tau values by deleting the inf values
Tau2_RT=Tau2_sort(1:NUM_tau); % RT
Tau3_ind=Tau3_sort(1:NUM_tau); % indices of omega
```

```
% create the matrix to save delay intervals (first two columns) and NU
% value (third column)
stability=zeros(NUM_tau,3);
stability(1,2)=Tau1_SORT(1); % initialize the first row of the matrix
for ii=2:NUM_tau % initialized the other rows of the matrix
   stability(ii,1)=Tau1_SORT(ii-1);
   stability(ii,2)=Tau1_SORT(ii);
end

% find NU distribution for each delay interval
stability(1,3)=NU_tau_zero; % initialize NU value for the first interval
for ii=2:NUM_tau % calculate the NU distributions for each interval
   if Tau2_RT(ii-1)==1
      stability(ii,3)=stability(ii-1,3)+2;
   else
      stability(ii,3)=stability(ii-1,3)-2;
   end
end

stability
% find the stability region (i.e. NU=0)
ind_stable=find(stability(:,3)==0); % find the index for which NU=0
Tau_stable=stability(ind_stable,1:2) % stable regions for the system

% NU vs T plot
```

```
figure(10);
stairs(stability(:,1),stability(:,3));


xlabel('\tau','FontWeight','bold','FontSize',30);
ylabel('NU','FontWeight','bold','FontSize',30);
% title('Superposed stability map','FontSize',25,'Fontweight','bold');
% set(legend,'FontWeight','bold','FontSize',20, 'FontName','Times New Roman')
handle=gca;
set(handle,'FontWeight','bold','FontSize',20, 'FontName','Times New Roman');
xlim([0,5]);
```

```
% Subroutine: sym2polys
function a = sym2polys(p,x)
%Sym2Polys  Extract the coefficients of a symbolic polynomial.
%          This function is an extension of the Matlab SYM2POLY and COEFFS
%          functions in that it allows the coefficients to be symbolic and
%          returns the full coefficient vector including the zero coefficients.
%
%Usage: c = sym2polys(p,x)
%       where p is the (multi) symbolic polynomial and x is the
%       independent variable. If x is not specified then the variable
%       alphabetically closest to x is used as the independent variable.
%
%Example:    If p = a*b*x^3 + b*c*x + c*d
```

```
%           then sym2polys(p) returns [a*b, 0, b*c, c*d]
%           whereas sym2polys(p,'b') returns [a*x^3+c*x, c*d]
%           Note that coeffs(p,x) returns [c*d, b*c, a*b]

%see also: sym2poly, coeffs

% Mukhtar Ullah
% mukhtar.ullah@informatik.uni-rostock.de
% September 2, 2004

if nargin == 1, x = findsym(p,1); end

[c,t] = coeffs(p,x);
i = sym2poly(sort(sum(t*(1:numel(t)).')));
a = sym(i);
a(i>0) = c(i(i>0));

if isempty(findsym(a)), a = double(a); end
```

```
% Subroutine: rouths
% This subroutine generates the rouths table from the polynomial
function R=rouths(C)
n=length(C);
```

```
%R=zeros(n,ceil(n/2));
R(1,:)=C(1:2:n);
R(2,1:length(2:2:n))=C(2:2:n);
for i=3:n
   for j=1:ceil(n/2)-1
      R(i,j)=(R(i-1,1)*R(i-2,j+1)-R(i-2,1)*R(i-1,j+1))/R(i-1,1);
   end
end
```

References

[1] G. Stépán, "Delay-differential equation models for machine tool chatter," *Dynamics and chaos in manufacturing processes,* vol. 471152935, pp. 165-192, 1998.

[2] R. Izmailov, "Analysis and optimization of feedback control algorithms for data transfers in high-speed networks," *SIAM journal on control and optimization,* vol. 34, pp. 1767-1780, 1996.

[3] R. Anderson and M. W. Spong, "Bilateral control of teleoperators with time delay," *Automatic Control, IEEE Transactions on,* vol. 34, pp. 494-501, 1989.

[4] R. Olfati-Saber and R. M. Murray, "Consensus problems in networks of agents with switching topology and time-delays," *Automatic Control, IEEE Transactions on,* vol. 49, pp. 1520-1533, 2004.

[5] N. Olgac, U. Zalluhoglu, and A. S. Kammer, "Predicting Thermoacoustic Instability: A Novel Analytical Approach and Its Experimental Validation," *Journal of Propulsion and Power,* vol. 30, pp. 1005-1015, 2014.

[6] G. Orosz, B. Krauskopf, and R. E. Wilson, "Bifurcations and multiple traffic jams in a car-following model with reaction-time delay," *Physica D: Nonlinear Phenomena,* vol. 211, pp. 277-293, 2005.

[7] S. A. Campbell, S. Ruan, G. Wolkowicz, and J. Wu, "Stability and bifurcation of a simple neural network with multiple time delays," *Fields Inst. Commun,* vol. 21, pp. 65-79, 1999.

[8] J. Chen, G. Gu, and C. N. Nett, "A new method for computing delay margins for stability of linear delay systems," in *Decision and Control, 1994., Proceedings of the 33rd IEEE Conference on*, 1994, pp. 433-437.

[9] K. L. Cooke and P. Van Den Driessche, "On zeroes of some transcendental equations," *Funkcialaj Ekvacioj*, vol. 29, pp. 77-90, 1986.

[10] J. K. Hale, *Theory of Functional Differential Equations*. New York: Springer-Verlag, 1977.

[11] S.-I. Niculescu, *Delay effects on stability: a robust control approach* vol. 269: Springer Science & Business Media, 2001.

[12] P. Park, "A delay-dependent stability criterion for systems with uncertain time-invariant delays," *IEEE Transactions on Automatic Control*, vol. 44, pp. 876-877, 1999.

[13] D. Breda, "On characteristic roots and stability charts of delay differential equations," *International journal of robust and nonlinear control*, vol. 22, pp. 892-917, 2012.

[14] D. Breda, S. Maset, and R. Vermiglio, "Pseudospectral differencing methods for characteristic roots of delay differential equations," *SIAM Journal on Scientific Computing*, vol. 27, pp. 482-495, 2005.

[15] E. A. Butcher, H. Ma, E. Bueler, V. Averina, and Z. Szabo, "Stability of linear time‐periodic delay‐differential equations via Chebyshev polynomials," *International Journal for Numerical Methods in Engineering*, vol. 59, pp. 895-922, 2004.

[16] K. Engelborghs, T. Luzyanina, and D. Roose, "Numerical bifurcation analysis of delay differential equations using DDE-BIFTOOL," *ACM Transactions on Mathematical Software (TOMS)*, vol. 28, pp. 1-21, 2002.

[17] K. Engelborghs and D. Roose, "On stability of LMS methods and characteristic roots of delay differential equations," *SIAM Journal on Numerical Analysis,* vol. 40, pp. 629-650, 2002.

[18] T. Insperger and G. Stépán, "Semi - discretization method for delayed systems," *International Journal for numerical methods in engineering,* vol. 55, pp. 503-518, 2002.

[19] D. J. Tweten, G. M. Lipp, F. A. Khasawneh, and B. P. Mann, "On the comparison of semi-analytical methods for the stability analysis of delay differential equations," *Journal of Sound and Vibration,* vol. 331, pp. 4057-4071, 2012.

[20] T. Vyhlídal and P. Zítek, "Mapping based algorithm for large-scale computation of quasi-polynomial zeros," *Automatic Control, IEEE Transactions on,* vol. 54, pp. 171-177, 2009.

[21] A. F. Ergenc, N. Olgac, and H. Fazelinia, "Extended Kronecker summation for cluster treatment of LTI systems with multiple delays," *SIAM Journal on Control and Optimization,* vol. 46, pp. 143-155, 2007.

[22] H. Fazelinia, R. Sipahi, and N. Olgac, "Stability robustness analysis of multiple time-delayed systems using “building block” concept," *Automatic Control, IEEE Transactions on,* vol. 52, pp. 799-810, 2007.

[23] M. E. Cavdaroglu and N. Olgac, "Full-state feedback control design with" delay scheduling" for cart-and-pendulum dynamics," in *Time Delay Systems,* 2009, pp. 296-302.

[24] A. F. Ergenc, H. Fazelinia, and N. Olgac, "Sign inverting control logic for time delayed systems, with experiments," *International Journal of Mechatronics and Manufacturing Systems,* vol. 1, pp. 68-82, 2008.

[25] K. Gu and M. Naghnaeian, "Stability crossing set for systems with three delays," *Automatic Control, IEEE Transactions on,* vol. 56, pp. 11-26, 2011.

[26] K. Gu, S.-I. Niculescu, and J. Chen, "On stability crossing curves for general systems with two delays," *Journal of Mathematical Analysis and Applications,* vol. 311, pp. 231-253, 2005.

[27] V. B. Kolmanovskiĭ, *Stability of functional differential equations* vol. 180: Elsevier, 1986.

[28] N. Olgac and R. Sipahi, "An exact method for the stability analysis of time delayed LTI systems," *IEEE Transactions on Automatic Control,* vol. 47, pp. 793-797, 2002.

[29] R. Sipahi and N. Olgac, "A unique methodology for the stability robustness of multiple time delay systems," *Systems & Control Letters,* vol. 55, pp. 819-825, 2006.

[30] H. Fazelinia, *A novel stability analysis of systems with multiple time delays and its application to high speed milling chatter*: University of Connecticut, 2007.

[31] J. K. Hale and W. Huang, "Global Geometry of the Stable Regions for Two Delay Differential Equations," *Journal of Mathematical Analysis and Applications,* vol. 178, pp. 344-362, 1993.

[32] Z. V. Rekasius, "A Stability Test for Systems with Delays," in *Proc. Joint Automatic Control Conf., Paper No. TP9-A,* 1980.

[33] Q. Gao, U. Zalluhoglu, and N. Olgac, "Investigation of Local Stability Transitions in the Spectral Delay Space and Delay Space," *Journal of Dynamic Systems, Measurement, and Control,* vol. 136, p. 051011, 2014.

[34] E. Jarlebring, "Critical delays and polynomial eigenvalue problems," *Journal of computational and applied mathematics,* vol. 224, pp. 296-306, 2009.

[35] J. Chen, G. Gu, and C. N. Nett, "A new method for computing delay margins for stability of linear delay systems," *Systems & Control Letters*, vol. 26, pp. 107-117, 1995.

[36] A. Packard and J. Doyle, "The complex structured singular value," *Automatica*, vol. 29, pp. 71-109, 1993.

[37] M. Spivak, "Calculus. Corrected," ed: Cambridge University Press, 2006.

[38] I. M. Gelfand, I. M. Gelfand, M. Kapranov, and A. Zelevinsky, *Discriminants, resultants, and multidimensional determinants*: Springer Science & Business Media, 2008.

[39] A. Dixon, "The eliminant of three quantics in two independent variables," *Proceedings of the London Mathematical Society*, vol. 2, pp. 49-69, 1909.

[40] D. Kapur, T. Saxena, and L. Yang, "Algebraic and geometric reasoning using Dixon resultants," in *Proceedings of the international symposium on Symbolic and algebraic computation*, 1994, pp. 99-107.

[41] G. E. Collins, "The calculation of multivariate polynomial resultants," in *Proceedings of the second ACM symposium on Symbolic and algebraic manipulation*, 1971, pp. 212-222.

[42] F. S. Macaulay and P. Roberts, *The algebraic theory of modular systems*: University press Cambridge, 1916.

[43] J. Canny and I. Emiris, "An efficient algorithm for the sparse mixed resultant," in *Applied algebra, algebraic algorithms and error-correcting codes*, ed: Springer, 1993, pp. 89-104.

[44] D. Kapur and T. Saxena, "Comparison of various multivariate resultant formulations," in *Proceedings of the 1995 international symposium on Symbolic and algebraic computation*, 1995, pp. 187-194.

[45] A. Cayley, "On the theory of elimination," *Cambridge and Dublin Math. J*, vol. 3, pp. 116-120, 1848.

[46] N. Olgac and R. Sipahi, "An improved procedure in detecting the stability robustness of systems with uncertain delay," *IEEE transactions on automatic control*, vol. 51, p. 1164, 2006.

[47] K. Ogata, *System dynamics* ed. 3: Prentice Hall Upper Saddle River, NJ, 1998.

[48] J. K. Hale and S. M. Verduyn Lunel, *An Introduction to Functional Differential Equations*. New York: Springer-Verlag, 1993.

[49] K. Gu, J. Chen, and V. L. Kharitonov, *Stability of time-delay systems*: Springer Science & Business Media, 2003.

[50] G. F. Franklin, J. D. Powell, and A. Emami-Naeini, "Feedback control of dynamics systems," *Pretince Hall Inc*, 2006.

[51] S. Jung, H.-T. Cho, and T. C. Hsia, "Neural network control for position tracking of a two-axis inverted pendulum system: Experimental studies," *Neural Networks, IEEE Transactions on*, vol. 18, pp. 1042-1048, 2007.

[52] X. Lu, F. Austin, and S. Chen, "Formation control for second-order multi-agent systems with time-varying delays under directed topology," *Communications in Nonlinear Science and Numerical Simulation*, vol. 17, pp. 1382-1391, 2012.

[53] Q. Gao, R. Cepeda-Gomez, and N. Olgac, "The Homicidal Chauffeur Problem with Multiple Time Delayed Feedback," in *Time Delay Systems*, 2012, pp. 97-101.

[54] Q. Gao, U. Zalluhoglu, and N. Olgac, "Equivalency of Stability Transitions Between the SDS (Spectral Delay Space) and DS (Delay Space)," in *ASME 2013 Dynamic Systems and Control Conference*, 2013, pp. V002T21A001-V002T21A001.

[55] Q. Gao, A. S. Kammer, U. Zalluhoglu, and N. Olgac, "Sign inverting and Delay Scheduling Control concepts with multiple rationally independent delays," in *American Control Conference (ACC), 2014*, 2014, pp. 5546-5551.

[56] Q. Gao, A. S. Kammer, U. Zalluhoglu, and N. Olgac, "Some critical properties of sign inverting control for LTI systems with multiple delays."

[57] Q. Gao, R. Cepeda-Gomez, and N. Olgac, "A test platform for cognitive delays: target tracking problem with multiple time-delayed feedback control," *International Journal of Dynamics and Control*, vol. 2, pp. 77-85, 2014.

[58] Q. Gao and N. Olgac, "Optimal sign inverting control for time-delayed systems, a concept study with experiments," *International Journal of Control*, vol. 88, pp. 113-122, 2015.

[59] W. Michiels and S.-I. Niculescu, *Stability and Stabilization of Time-Delay Systems (Advances in Design & Control)(Advances in Design and Control)*: Society for Industrial and Applied Mathematics, 2007.

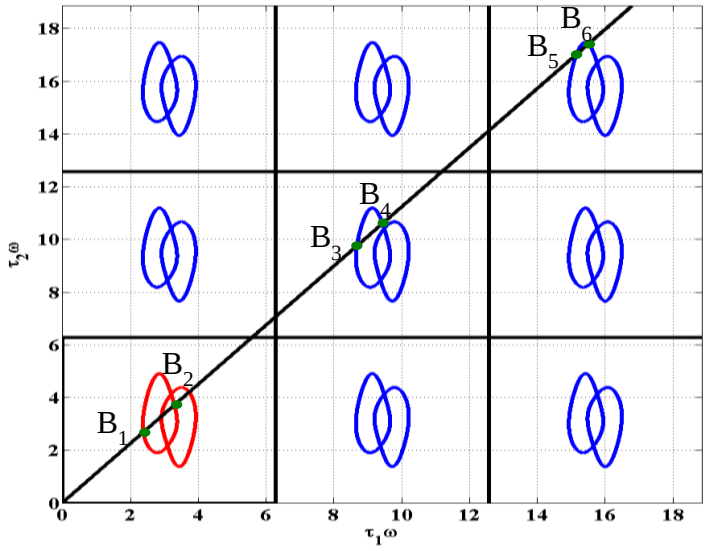

Fig. 1. Spectral delay space (SDS) representation of the example case study in Section 2.2.4

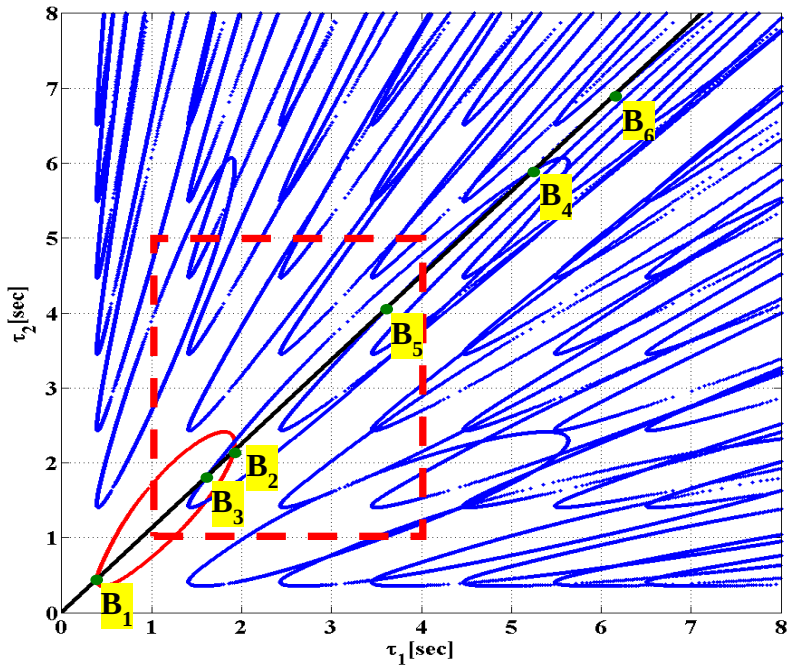

Fig. 2. (τ_1, τ_2) delay space (DS) representation of the example case study in Section 2.2.4

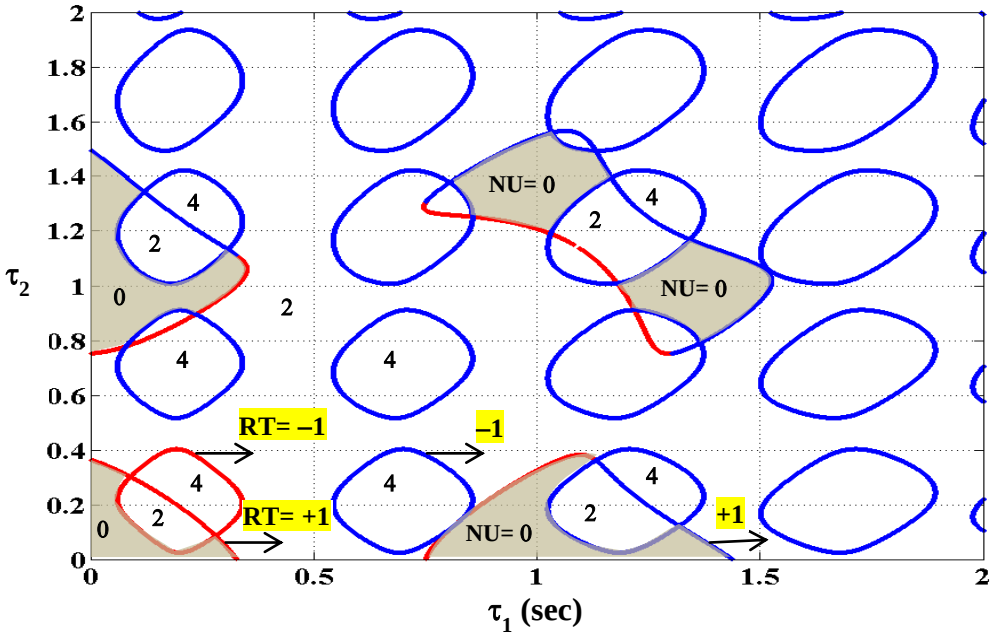

Fig. 3. Stability map of the example case in Section 2.3.4 for τ_3=0.5 second, τ_4=1.5 seconds, τ_5=1 second; Shaded regions are stable; Red and blue curves are KH and OH, respectively.

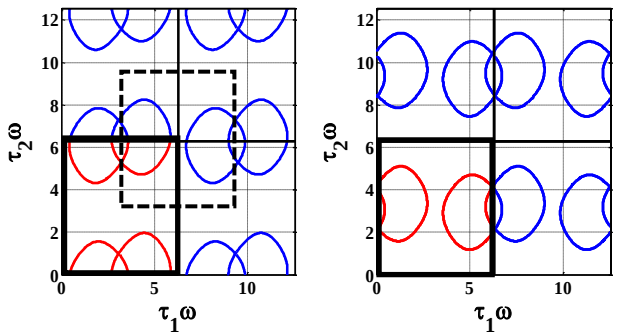

Fig. 4. Spectral Delay Space (SDS) representations of the original (left) and inverted (right) systems in Section 3.5. BB is marked in dark with building hypersurface (red) within.

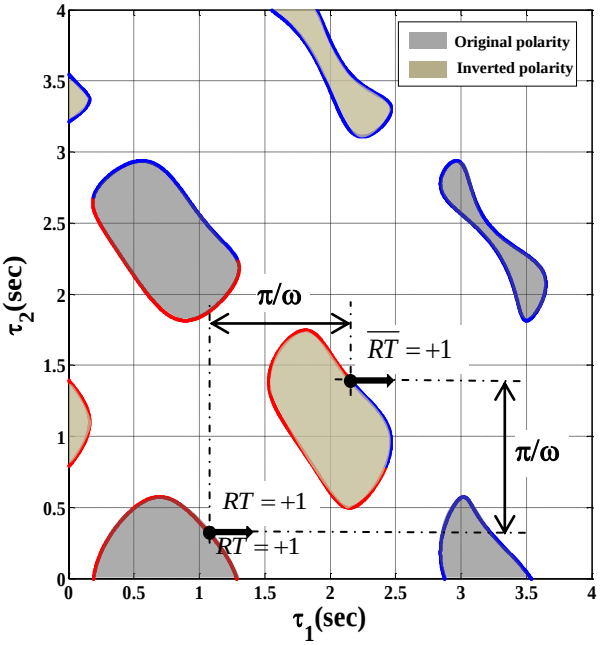

Fig. 5. Combined stability map with kernel (red) and offspring (blue) hypersurfaces for the example in Section 3.5.

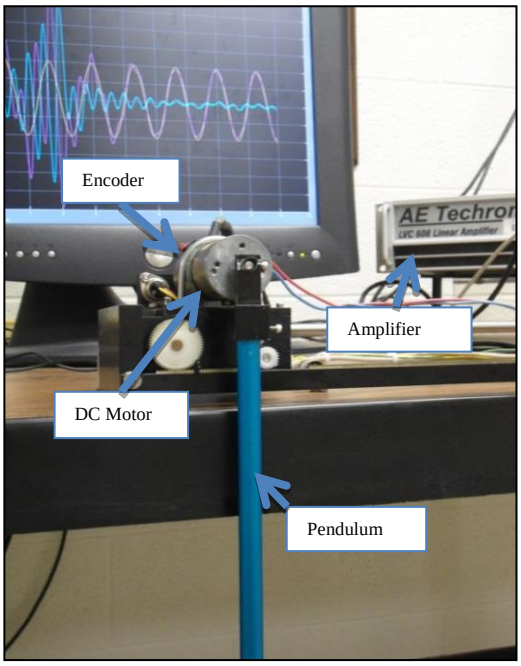

Fig. 6. Experimental setup in Section 5.

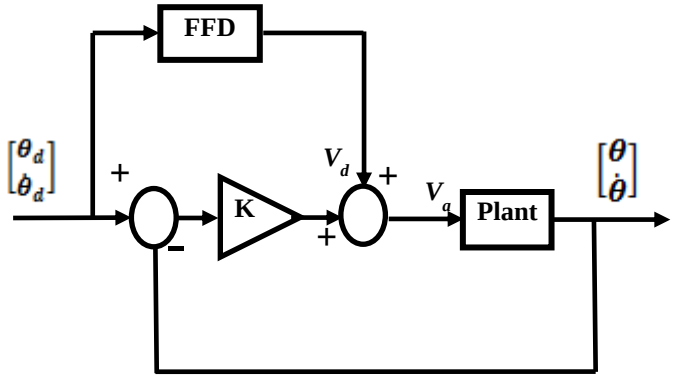

Fig. 7. Feed-forward and feedback control structure in Section 5.

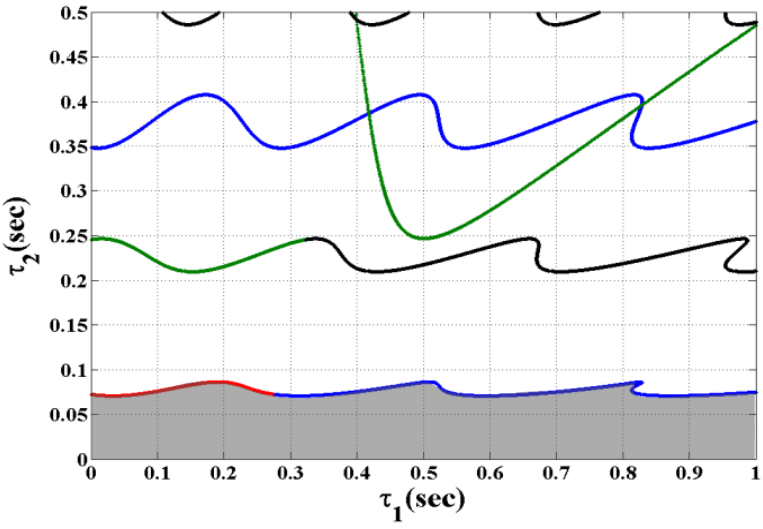

Fig. 8. Superposed stability map for original and SIC controls when α=1. SIC does not offer stable region.

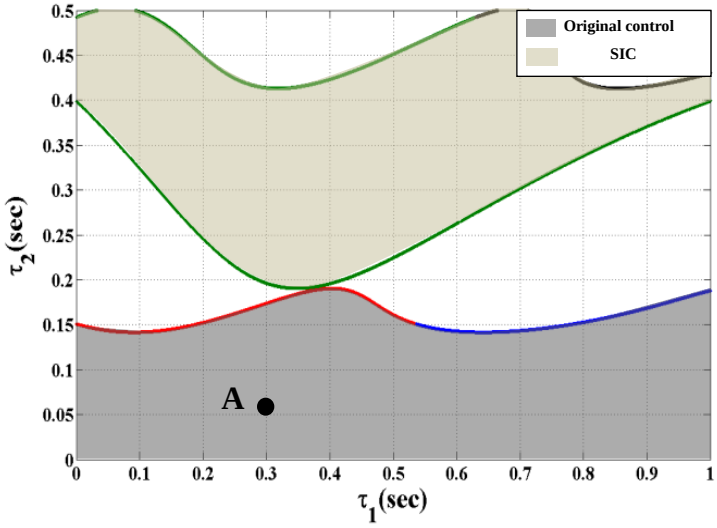

Fig. 9. Superposed stability maps for original and SIC cases when α=0.35. Shaded regions are stable.

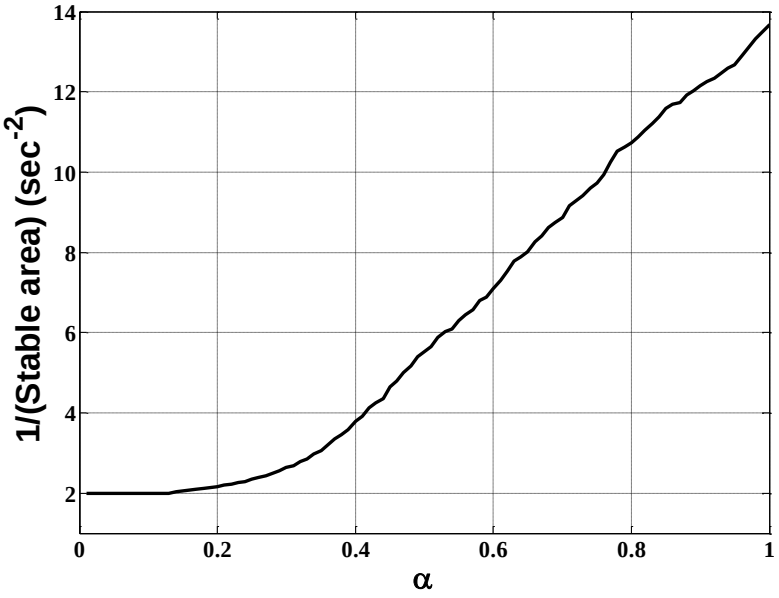

Fig. 10. $(Area_{stable})^{-1}$ variation as a function of α.

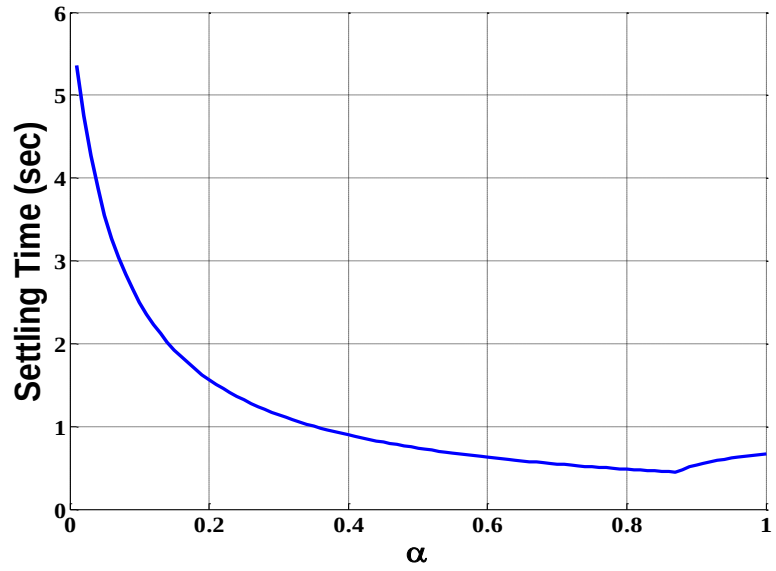

Fig. 11. Settling time variation for the non-delayed dynamics as in (5.3) as a function of α.

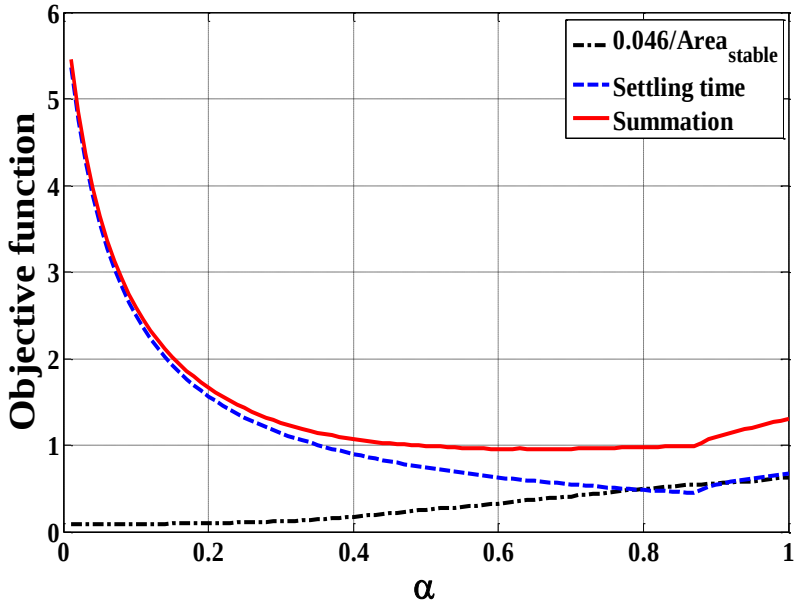

Fig. 12. Objective function.

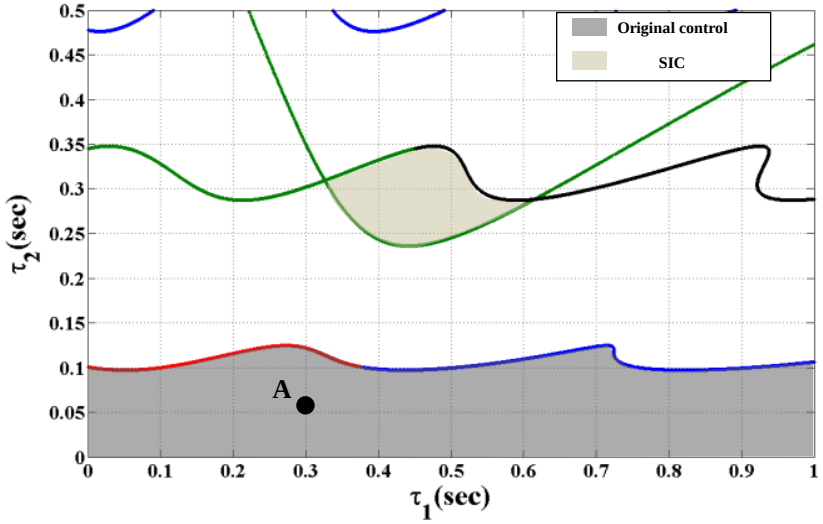

Fig. 13. Superposed stability map for the characteristic Eq. (12) when α^{*}=0.65. Shaded regions are stable.

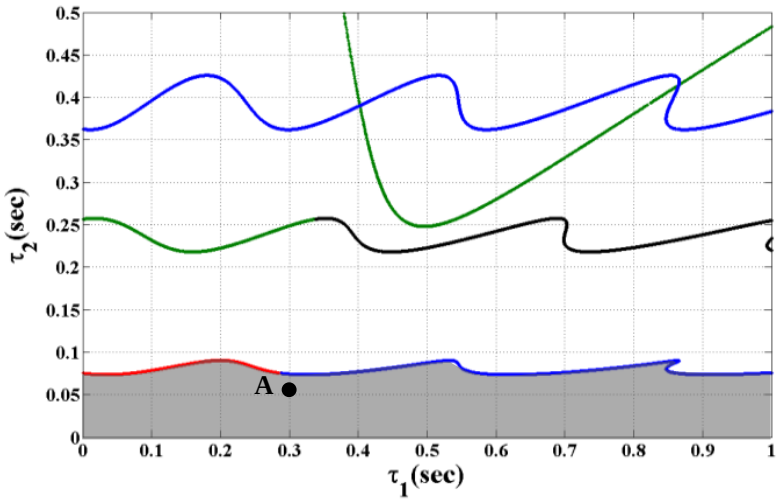

Fig. 14. Superposed stability map for the characteristic Eq. (12) when α=0.95. The shaded region is stable.

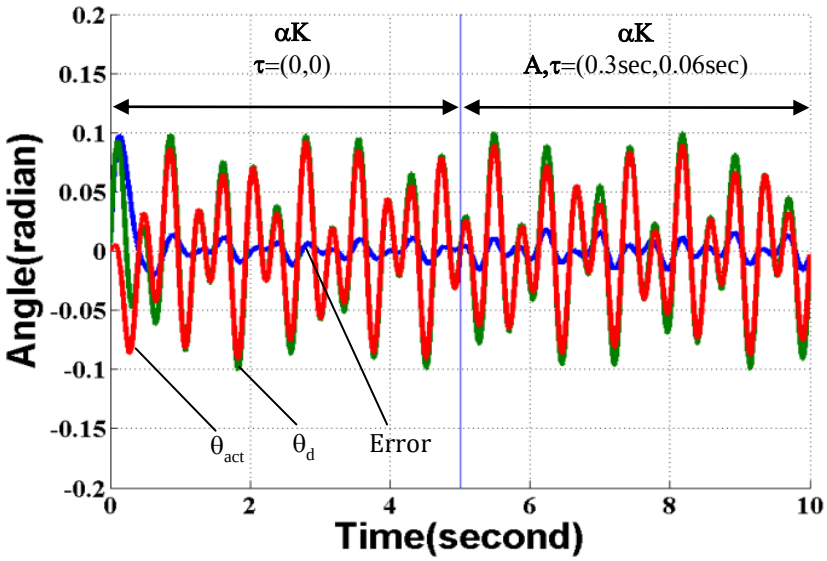

Fig. 15. Tracking performance when α = 0.35.

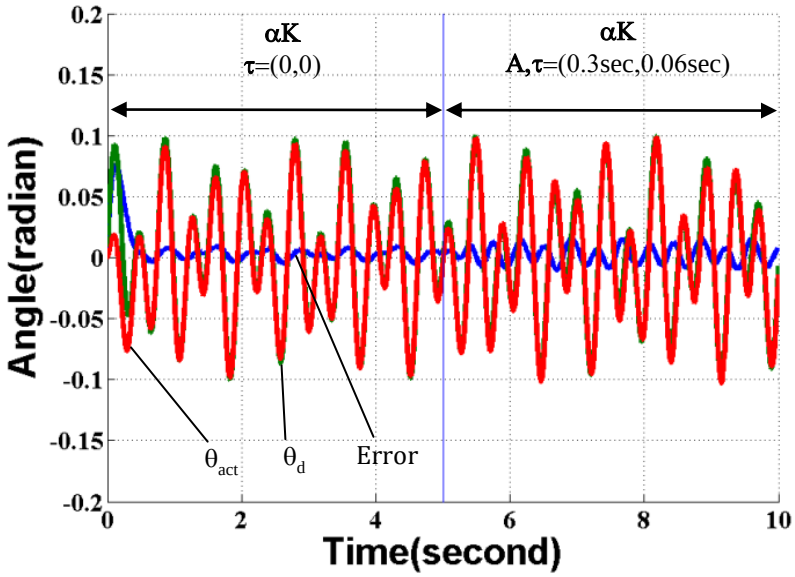

Fig. 16. Tracking performance when $\alpha^* = 0.65$.

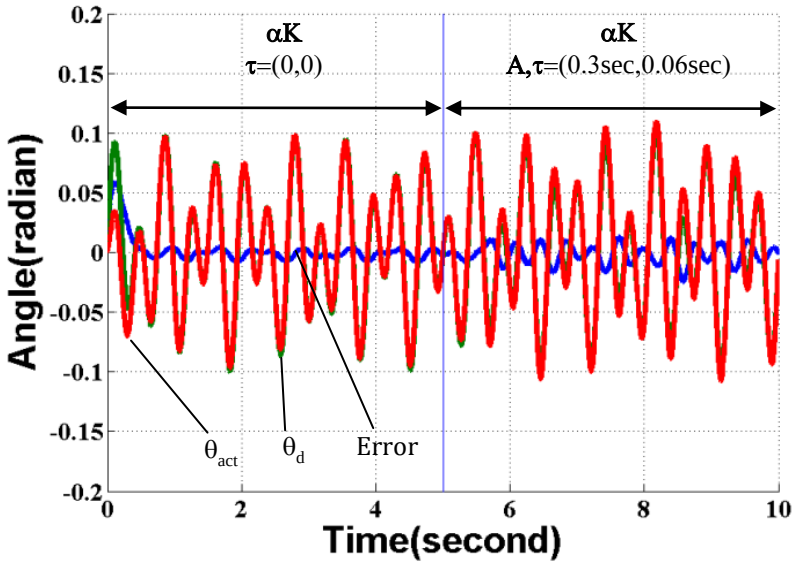

Fig. 17. Tracking performance when $\alpha = 0.95$.